Stable Isotope Labeling with Amino Acids in Cell Culture (SILAC)-based Quantitative Proteomics Study of a Thyroid Hormone-regulated Secretome in Human Hepatoma Cells*[S]

Cheng-Yi Chen‡, Lang-Ming Chi§, Hsiang-Cheng Chi‡, Ming-Ming Tsai‡¶, Chung-Ying Tsai‡, Yi-Hsin Tseng‡, Yang-Hsiang Lin‡, Wei-Jan Chen‖, Ya-Hui Huang, and Kwang-Huei Lin‡ ‡‡**

The thyroid hormone, 3, 3′,5-triiodo-L-thyronine (T_3), regulates cell growth, development, differentiation, and metabolism via interactions with thyroid hormone receptors (TRs). However, the secreted proteins that are regulated by T_3 are yet to be characterized. In this study, we used the quantitative proteomic approach of stable isotope labeling with amino acids in cell culture coupled with nano-liquid chromatography-tandem MS performed on a LTQ-Orbitrap instrument to identify and characterize the T_3-regulated proteins secreted in human hepatocellular carcinoma cell lines overexpressing TRα1 (HepG2-TRα1). In total, 1742 and 1714 proteins were identified and quantified, respectively, in three independent experiments. Among these, 61 up-regulated twofold and 11 down-regulated twofold proteins were identified. Eight proteins displaying increased expression and one with decreased expression in conditioned media were validated using Western blotting. Real-time quantitative RT-PCR further disclosed induction of plasminogen activator inhibitor-1 (PAI-1), a T_3 target, in a time-course and dose-dependent manner. Serial deletions of the *PAI-1* promoter region and subsequent chromatin immunoprecipitation assays revealed that the thyroid hormone response element on the promoter is localized at positions –327/–312. PAI-1 overexpression enhanced tumor growth and migration in a manner similar to what was seen when T_3 induced PAI-1 expression in J7-TRα1 cells, both *in vitro* and *in vivo*. An *in vitro* neutralizing assay further supported a crucial role of secreted PAI-1 in T_3/TR-regulated cell migration. To our knowledge, these results demonstrate for the first time that proteins involved in the urokinase plasminogen activator system, including PAI-1, uPAR, and BSSP4, are augmented in the extra- and intracellular space of T_3-treated HepG2-TRα1 cells. The T_3-regulated secretome generated in the current study may provide an opportunity to establish the mechanisms underlying T_3-associated tumor progression and prognosis. ***Molecular & Cellular Proteomics 11: 10.1074/mcp.M111.011270, 1–19, 2012.***

The thyroid hormone (TH)[1], a pleiotropic regulator of growth, differentiation, proliferation and many other physiological processes, acts via interactions with thyroid hormone response elements (TREs) in the regulatory regions of target genes (1). Cheng and co-workers have reported AGGTCA as a putative consensus hexamer half-site sequence of TRE (1). The TREs are arranged as direct repeats (DR), palindromes, and inverted palindromes (IP), and display considerable variations in nucleotide sequences, spacing, number, and orientation of half-sites (1–3). The amino acid sequences of thyroid hormone receptors (TRs) are highly homologous with those of

From the ‡Department of Biochemistry, School of Medicine, Chang-Gung University, Taoyuan, Taiwan 333; §Molecular Medicine Research Center, School of Medicine, Chang-Gung University, Taoyuan, Taiwan 333; ¶Department of Nursing, Chang-Gung University of Science and Technology, Taoyuan, Taiwan 333; ‖First Cardiovascular Division, Chang Gung Memorial Hospital, Taoyuan, Taiwan 333; **Medical Research Central, Chang Gung Memorial Hospital, Taoyuan, Taiwan 333

Received May 30, 2011, and in revised form, December 12, 2011
Published, MCP Papers in Press, December 14, 2011, DOI 10.1074/mcp.M111.011270

[1] The abbreviations used are: TH, thyroid hormone; TRs, thyroid hormone receptors; SILAC, stable isotope labeling with amino acid in cell culture; HCC, hepatocellular carcinoma; TRE, thyroid hormone response element; RXR, retinoid X receptor; SMRT, silencing mediator of retinoic and thyroid receptor; NCoR, nuclear receptor corepressor; DR, direct repeat; IP, inverted palindromes; GeLC-MS/MS, one-dimensional SDS-PAGE in conjugation with nano-LC-MS/MS; 2DLC-MS/MS, two-dimensional LC-MS/MS; LC, liquid chromatography; SCX, strong cation exchange; RP18, reverse phase 18; TMHMM, transmembrane hidden Markov model; FINC, fibronectin; FURIN, furin; GELS, gelsolin; PAI-1, plasminogen activator inhibitor-1; MMPs, matrix metalloproteinases; uPAR, urokinase plasminogen activator surface receptor; BSSP4, brain-specific serine protease 4; CATH, cathepsin H; uPA, urokinase plasminogen activator; H&E, hematoxylin and eosin; IHC, immunohistochemistry.

steroid hormone receptors (2, 4). TRs are ligand-dependent transcription factors that consist of modular function domains that mediate DNA binding, hormone binding (ligands), receptor homo- and heterodimerization, and interaction with other transcription factors and cofactors (5, 6).

TRs interact with retinoid X receptor (RXR) and form heterodimers that influence target genes via binding to TREs located in the regulatory regions (7, 8). TH-bound TRs activate target gene expression. In contrast, gene expression is repressed by non-T_3-bound TRs. Unliganded TRs act as repressors by recruiting corepressors, such as silencing mediator of retinoic and thyroid receptor (SMRT) and nuclear receptor corepressor (NCoR), as a result of altered conformations upon binding to TREs. Conversely, binding of T_3 to TRs causes conformational changes and subsequent recruitment of multiple coactivator complexes (1, 5). Two TR genes, *TR*α and *TR*β, have been identified on human chromosomes 17 and 3, respectively (5, 9). TRα1, TRα2, TRβ1 and TRβ2 isoforms are generated via alternative splicing and promoter usage of the primary transcript (10). The liver is the typical target organ of the thyroid hormone, and equivalent expression levels of TRα1 and TRβ1 have been reported in human hepatocytes (11).

Previous microarray analysis experiments by our group have demonstrated that numerous genes including coagulation factor system components (12), plasma proteins (12, 13), nuclear receptor coactivator (14), antimetastatic proteins (15), proteases (16), and oncogenes (17) are regulated by T_3. Additionally, we have identified several T_3-regulated extracellular proteins such as matrix metalloproteinases (MMPs) and cysteine cathepsins. These proteases are involved in cellular processes and intercellular communication during cancer progression and development (18–20). It implied that T_3 may have a role in the regulation of secreted proteins. Recently, proteomics approach has been successfully applied to investigate the regulatory secreted proteins systemically (secretome) of tumor-associated genes (21–25). Herein, we applied the stable isotope labeling with amino acids in cell culture (SILAC)-based quantitative proteomic approaches to identify secreted proteins regulated by T_3 and study their underlying physiological significance in hepatoma cell lines stably expressing wild-type TR.

Plasminogen activator inhibitor-1 (PAI-1), a T_3 target, elevated levels in the tumor microenvironment is associated with high mortality and poor prognosis of patients with many forms of cancer (26). In the present study, we focused on the potential role played by PAI-1 after T_3 induction.

EXPERIMENTAL PROCEDURES

Cell Culture—Human hepatoma cells, HepG2, Huh7, J7, and Mahlavu were routinely cultured at 37 °C in a humidified atmosphere of 95% air and 5% CO_2 in Dulbecco's modified Eagle's medium (DMEM) supplemented with 10% fetal bovine serum (FBS). HepG2 and J7 cell lines were stably transfected with TRα1 (HepG2-TRα1#1, HepG2-TRα1#2, and J7-TRα1) or TRβ1 (HepG2-TRβ1). The vector control cell line employed was HepG2-Neo (16, 17). Huh7-PAI-1 represents the Huh7 cell line overexpressing PAI-1. Serum was depleted of T_3 (Td), as described previously (27). For SILAC experiments, human HepG2-TRα1 cells were maintained in SILAC medium comprising DMEM (Invitrogen, Carlsbad, CA) supplemented with 10% dialyzed fetal bovine serum (Invitrogen), L-lysine and L-arginine (Sigma-Aldrich) or [$^{13}C_6$]-L-lysine, [$^{13}C_6$]-L-arginine (Isotec) added at a concentration of 0.1 g/L for light or heavy stable isotope labeling (28). Both light and heavy isotope-labeled HepG2-TRα1 cells were maintained for at least 10 doubling times to achieve $>$ 95% incorporation of labeled amino acid.

Preparation of Conditioned Medium and In-solution Protein Digestion—Cells were passaged and differentiated as described above. HepG2-TRα1 cells were grown to confluence in 10-cm cell culture dishes. The cells contacting dishes were washed twice with phosphate-buffered saline (PBS) to reduce the amount of contaminating protein in serum (29). Cells were incubated in serum-free medium and either treated with T_3 or left untreated for 24 h. At the end of the treatment period, conditioned media (CM) were collected and centrifuged at 1500 $\times$ *g* to eliminate intact cells following concentration using spin columns with a molecular mass cut-off of 3 kDa (Amicon Ultra, Millipore, Billerica, MA). Equal amounts of proteins were mixed for quantitative proteomic analysis (28).

Preparation of Tryptic Peptides in Solution—Mixed SILAC proteins were reduced and alkylated with 5 mM dithiothreitol for 60 min and 10 mM iodoacetamide for 60 min, followed by digestion with sequencing grade-modified trypsin (1:25, w/w) (Promega, Madison, WI) at 37 °C overnight. The digestion reaction was terminated by adding formic acid at a concentration of 0.1%.

Two-Dimensional Liquid Chromatography (2D-LC) Separation—Peptides prepared from in-solution digestion were separated and analyzed via the online 2D LC-MS/MS technique using strong cation exchange (SCX) and reverse-phase 18 (RP18) nanoscale liquid chromatography coupled with LTQ-Orbitrap mass spectrometry (Thermo Electron, Bremen, Germany) (30). Briefly, equally mixed SILAC peptides were injected into an in-house packed SCX column (Luna SCX, 5 μm, 0.5 $\times$ 150 mm; Phenomenex, Torrance, CA) and fractionated into 45 fractions using a continuous ammonium chloride gradient in the presence of 30% acetonitrile and 0.1% formic acid. Each SCX fraction was trapped on a RP18 column (Source 15 RPC, 0.5 $\times$ 5 mm, GE) and separated using coupled BEH RP18 chromatography (1.7 μm, 0.1 $\times$ 120 mm; Waters, Milford, MA) with an acetonitrile gradient in 0.1% formic acid performed on a Dionex UltiMate 3000 nanoLC system.

One-dimensional Gel Electrophoresis Combined with Nanoliquid Chromatography (GeLC)—Proteins separated using SDS/PAGE were cut out of the gel and divided into 60 fractions for subsequent in-gel digestion (31). Peptides were analyzed with LC-MS/MS using nanoscale RP18 liquid chromatography coupled with LTQ-Orbitrap mass spectrometry. Briefly, peptides were trapped on a Zorbax 300SB RP18 column (0.3 $\times$ 5 mm, Agilent Technologies) and separated using a PicoFrit BioBasic C18 capillary column (0.075 $\times$ 120 mm; New Objective, Woburn, MA) with an acetonitrile gradient in 0.1% formic acid on a Surveyor HPLC system (Thermo Electron, Bremen, Germany).

Tandem Mass Spectrometry (MS/MS)—MS/MS analysis was performed on a LTQ-Orbitrap mass spectrometer (Thermo Fisher, San Jose, CA) with a nanoelectrospray ion source (Proxeon Biosystem). Full-scan MS spectra (m/z 430 - m/z 2000) were acquired in the Orbitrap mass analyzer at a resolution of 60,000 at *m/z* 400. The lock mass calibration feature was enabled to improve mass accuracy. The most intense ions (up to 12) with minimal signal intensity of 20,000 were sequentially isolated for MS/MS fragmentation in the order of intensity of precursor peaks in the linear ion trap using collision-

induced dissociation energy of 35%, Q activation at 0.25, activation time of 30 ms, and isolation width of 2.0. Targeted ions with $m/z \pm 30$ ppm were selected for MS/MS once (2D-LC) or twice (GeLC), and dynamically excluded for 50 (2D-LC) or 180 s (GeLC).

Protein Identification and Quantification in Shotgun Proteomics—All MS and MS/MS data were analyzed and processed with Quant.exe in MaxQuant environment (version 1.0.13.8) for peptide identification and quantification analyses as described before (32). Top six of fragment ions per 100 Da were extracted for a protein database search using the Mascot search engine (version 2.2.2, Matrix Science) against the concatenated Swiss-Prot version 56 human forward and reverse protein sequence data set with a set of common contaminant proteins (total 45500 entries). The search parameters were set as follows: Carbamidomethylation (C) as the fixed modification, oxidation (M), *N*-acetyl (protein) and pyro-Glu/Gln (N-term) as variable modifications, 7 ppm for MS tolerance, 0.5 Da for MS/MS tolerance, and 2 for missing cleavage. The SILAC label (K) (R) was set as none, fix or variable modification to generate three Mascot search results. The identified peptides and proteins in all search results were further analyzed in Identity.exe with following criteria: six for minimum peptide length, two for minimum unique peptides for the assigned protein. The posterior error probability of peptides identified in forward and reversed databases was used to rank and determine the false discovery rate for statistical evaluation (32, 33). We accepted the peptide and protein identifications with false discovery rate less than 1%. For protein quantification, we considered the protein with at least two ratio counts generated from unique and razor peptides. The median value of the SILAC ratios was calculated as protein abundance (H/L ratio) to minimize the effect of outlier values. The peptides shared (not unique for leading proteins) between multiple leading proteins were assigned to one of them (the first one) as razor peptides (the detail information was summarized in supplementary Table S2). Finally, the global median normalization was applied to recalculate the protein abundance (the normalized protein ratio) to reduce the system error from sample preparation in each experiment.

Network Analysis of Protein Secretion Mechanisms and Functions—Differentially expressed proteins identified from the three experiments were uploaded and analyzed with the GeneGo pathway maps tool of MetaCore™, Version 6.5 build 27009 (GeneGo, St. Joseph, MI). The secretion mechanisms of proteins were analyzed using the SignalP 3.0 program with a hidden Markov model to predict the presence of secretory signal peptide sequences (34), signifying the classical secretory pathway. Additionally, the SecretomeP 2.0 program was employed to predict nonsignal peptide-triggered protein secretion (35), representing a nonclassical secretory pathway, and TMHMM 2.0 to predict transmembrane helices in proteins (36).

Immunoblot Analysis—Total cell lysates and conditioned media were prepared, and protein concentrations determined with the Bradford assay kit (Pierce Biotechnology, Rockford, IL). Equivalent amounts of proteins were fractioned on a 10% sodium dodecyl sulfate (SDS)-polyacrylamide gel. Separated proteins were transferred to a nitrocellulose membrane (PH 7.9, Amersham Biosciences Inc., Piscataway, NJ), blocked with 5% nonfat powdered milk, incubated with a specific primary antibody at 4 °C overnight, and hybridized with the respective secondary antibody, HRP-conjugated mouse/rabbit/goat anti-IgG, for 1 h at room temperature. Finally, immune complexes were visualized using the chemiluminescence method with an ECL detection kit (Amersham Biosciences) on Fuji x-ray films, as described previously (37).

Quantitative Reverse Transcription Polymerase Chain Reaction (Q-RT-PCR)—Total RNA was extracted from T_3-treated HepG2-TRα1 cells using TRIzol reagent, as described previously (38). Subsequently, cDNA was synthesized via RT-PCR with the SuperscriptIIkit (Invitrogen, Karlsruhe, Germany). Real-time Q-RT-PCR was performed on a 15 μl reaction mixture containing 750 nM forward and reverse primers, varying amounts of template and 1 × Sybr Green reaction mix (Applied Biosystems, Foster City, CA). Sybr Green fluorescence was determined with the ABI PRISM 7500 detection system (Applied Biosystems). Primers were designed using Primer Express Software (Applied Biosystems). Genes were normalized against the control ribosomal binding protein (*RiboL35A*) gene. The human PAI-1 oligonucleotides used in this study included the forward primer, 5′-GCACAACCCCACAGGAACA-3′, and reverse primer, 5′-GTCCCAGATGAAGGCGTCTTT-3′.

Cloning and Activities of PAI-1 Promoter Fragments—Fragments of the *PAI-1* promoter (positions −2261 to +1203) were ligated into the pGL2 vector (Promega Corp., Madison, WI), based on the published sequence. Several serial deletion and mutation constructs of the *PAI-1* promoter were amplified via PCR and cloned into the pA3TK vector. The constructed promoter sequences were confirmed using automatic DNA sequencing. HepG2-TRα1 cells treated with 10 nM T_3 for 24 h were cotransfected with 0.6 μg DNA/well of pA3TK vector containing the *PAI-1* promoter sequence and 0.3 μg of SVβ plasmid, a β-galactosidase expression vector (Clontech, Palo Alto, CA), in 24-well plates using the TurboFect in transfection reagent (Fermentas, Glen Burnie, MD) to determine the transcriptional activities of TREs within the *PAI-1* promoter. At the end of the treatment period, transfected and non-transfected cells were lysed, and luciferase and β-galactosidase activities measured. Luciferase activity was normalized against that of β-galactosidase, as described earlier (39).

Chromatin Immunoprecipitation (ChIP) Assay—ChIP assays were performed to examine the interactions between TR and TRE on the *PAI-1* promoter (37). HepG2-TRα1 cells treated with 10 nM T_3 for 24 h or left untreated were harvested and cross-linked with 1% formaldehyde for 10 min at room temperature in medium. The reactions were terminated by adding 0.125 M glycine. Subsequently, cell lysates were washed with PBS three times and resuspended in lysis buffer (150 mM NaCl, 5 mM EDTA, 50 mM Tris (pH 8.0), 0.1% SDS and 0.1% sodium deoxycholate) containing three protease inhibitors (1 mM phenylmethylsulfonyl fluoride, aprotinin, and leupeptin). Cell lysates were sonicated with a Misonix Sonicator 3000 Homogenizer (Mandel Scientific Company Inc., Guelph, ON, Canada) to disrupt chromatin. Sonicated DNA was between 200 and 1000 bp in length. The products were precleared with 60 μl protein A/G agarose (Sigma Chemicals) for 2 h at 4 °C. Complexes were immunoprecipitated with anti-TR (kindly provided by the laboratory of Dr. S-Y Cheng at the National Cancer Institute), anti-RXRα (Santa Cruz Biotechnology, Santa Cruz, CA) and anti-IgG antibody (R&D Systems, Inc., Minneapolis, MN). The 100 bp fragments of *PAI-1* promoter containing the predicted TRE region were amplified via PCR with the forward primer, 5′-CCCAAGCTTCAGTCAACCTGGCAGGACAT-3′, and reverse primer, 5′-CCGCTCGAGGAACAATTGAGCAAACCCCAATA-3′.

Zymography Assay for Matrix Metallopeptidase MMP2 and MMP9—Huh7-PAI-1 and Huh7-control cells (5×10^6) were cultured in DMEM with 10% FBS. After 24 h of seeding, cells were washed twice with PBS and continuously incubated in serum-free medium for 24 h. Subsequently, conditioned media (CM) were collected and centrifuged at 1500 × *g* to eliminate intact cells followed by concentration using a spin column with a molecular mass cut-off of 3 kDa (Amicon Ultra, Millipore). Concentrated conditioned media (50 μg) were mixed with 50 mM Tris-HCl, pH 8.0, without reducing agent, and fractioned using 10% SDS-PAGE in the presence of 1 mg/ml gelatin. Following electrophoresis, the gel was washed with Zymogram Renaturing Buffer containing 2.5% Triton X-100 for 30 min twice at room temperature and incubated with Zymogram Developing Buffer (40 mM Tris-HCl, pH 8.0, 0.01% NaN3, 10 mM $CaCl_2$) at 37 °C overnight. Gels were stained with Coomassie brilliant blue R-250 and destained in 5% methanol and 7.5% acetic acid solution until the appearance of clear bands.

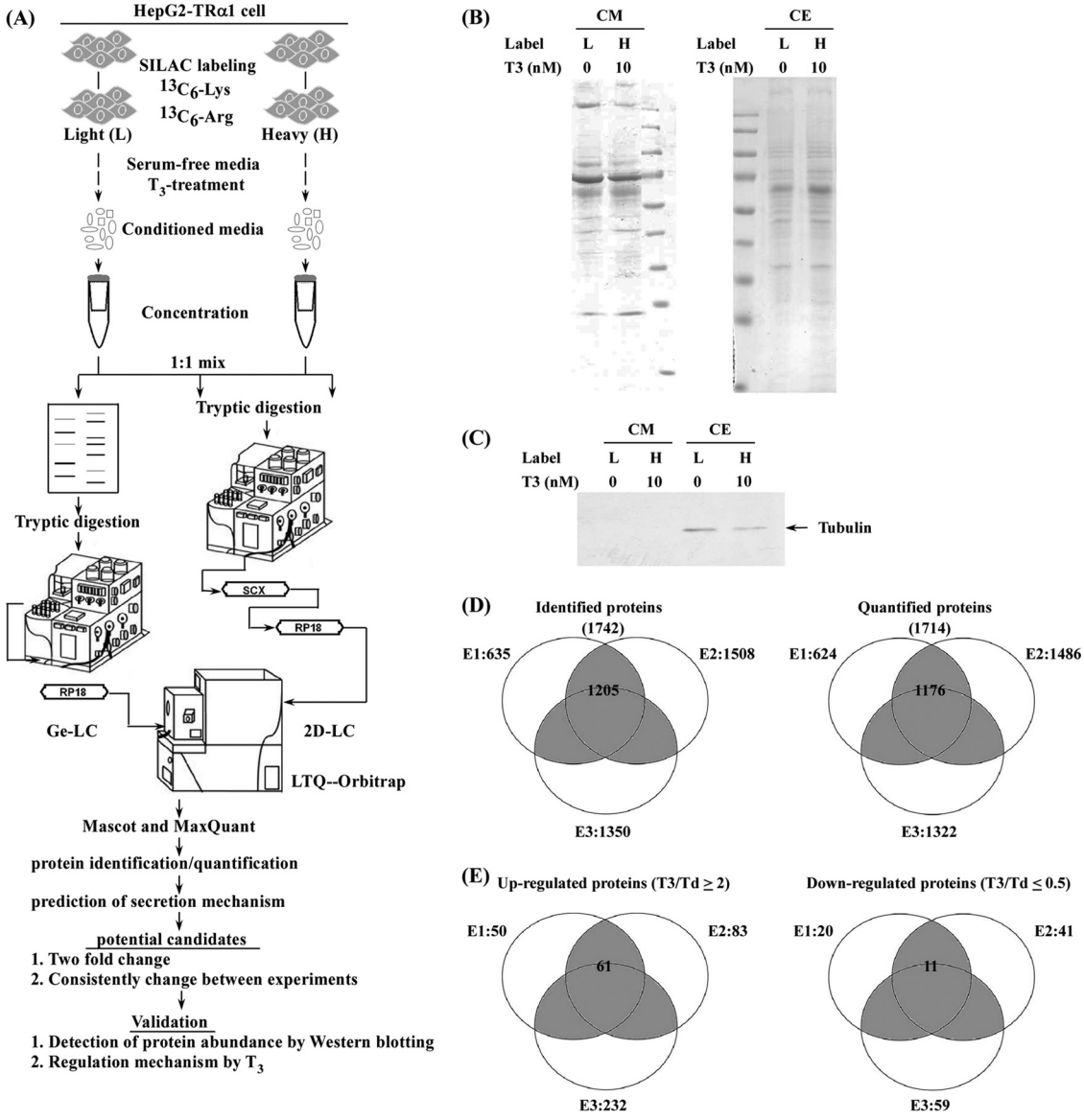

FIG. 1. **SILAC-based identification and quantification of the TH-regulated secretome.** *A*, Schematic diagram of SILAC-based protein identification and quantification of the T_3/TR-regulated secretome. The process included SILAC labeling, conditioned media collection, GeLC-MS/MS or 2DLC-MS/MS analysis, protein identification and quantification with Mascot and MaxQuant, and validation. *B*, Conditioned media and cell extracts (L: light, H: heavy) were resolved with 12% SDS-PAGE and stained with Coomassie blue. *C*, Proteins (20 μg) from the cell extracts and conditioned media were analyzed by Western blotting using the β-tubulin antibody. *D*, Venn diagrams depict the proteins identified and quantified in each SILAC-based experiment (E1, E2, E3). The total number of proteins identified or quantified in the three experiments is listed in brackets. The number in the gray area represents proteins identified or quantified in at least two experiments. *E*, The Venn diagrams show proteins up-regulated (T_3/Td $\geq$2) or down-regulated (T_3/Td $\leq$0.5) in the three SILAC-based experiments. The total number of up-regulated (T_3/Td $\geq$2) or down-regulated (T_3/Td $\leq$0.5) proteins in each experiment is labeled next to the corresponding circle. The numbers of up-regulated and down-regulated candidates detected in at least two of the experiments labeled in the gray area were analyzed with MetaCore software.

Cell Proliferation Assay—Cell proliferation rates were examined using the 3-(4,5-dimethylthiazol-2-yl)- 2,5-diphenyltetrazolium bromide (MTT; Promega) assay. Cells (4×10^3) were seeded on 48-well culture plates and harvested at 1–7 days. After overnight incubation, 150 μl MTT solution (10$\times$ dilution of 5 mg/ml MTT in DMEM without serum) was added to each well for 3 h at 37 °C, and 150 μl lysis buffer (6 M HCL and 10% SDS) subsequently added to solubilize formazan crystals at 37 °C overnight. Finally, absorbance at 570 nm was measured using a SpectraMax microplate reader. Absorbance at 570 nm was normalized against background absorbance at 650 nm.

Cloning of PAI-1—Total RNA (1 μg) was reverse-transcribed using Superscript II reverse transcriptase (Invitrogen) and Oligo (dT) to synthesize template cDNA. PAI-1 cDNA was amplified via PCR with the forward primer, 5′-CCGGAATTCATGCAGA TGTCTCCAGCCCT-3′, and reverse primer, 5′-CCGCTCGAGTCAGGGTTC CATCACT-TGGC-3′, for 30 cycles at 95 °C for 1 min, 60 °C for 1 min and 72 °C for 2 min. The PAI-1 open reading frame was ligated into pcDNA 3.0 expression vector, and the resulting construct sequenced.

Establishing a Huh7 Cell Line Stably Overexpressing PAI-1—The Huh7 cell line was transfected with the PAI-1 cDNA construct on 10

TABLE I
Proteins identified in the conditioned media of HepG2-TRα1 were predicted secretory pathways

Experiment	Number of identified proteins				Total protein	% of potentially secreted proteins
	Classical[a] secretion	Nonclassical[b] secretion	Membrane[c] protein	Others[d]		
E1	184	165	6	280	635	55.9
E2	360	405	18	725	1508	51.9
E3	349	365	17	619	1350	54.2
E1+E2+E3	399	484	26	833	1742	52.2

[a] Proteins were secreted via the classical secretory pathway using the SignalP software (SignalP probability ≥0.90).
[b] Proteins predicted by the secretomeP program to be secreted via the nonclassical secretory pathway (SignlP probability ≤0.90 and SecretomeP score ≥0.50).
[c] Proteins predicted via the TMHMM to form trans-membrane proteins that were not predicted to be secreted via the classical and nonclassical secretory pathway.
[d] Proteins predicted were not secreted via the classical pathway, nonclassical pathway and trans-membrane proteins.

cm cell culture dishes using Lipofectamine Reagent (Invitrogen). After 24 h, transfected cells were transferred to medium containing G418 (400 μg/ml) for selection until the generation of a single-cell clone. Expression of PAI-1 in Huh7 cells was confirmed by Western blotting.

In Vitro Migration and Invasion Assays—The influence of T_3 on PAI-1-mediated invasive activities of HepG2-TRα1 and Huh7-PAI-1 cells was determined with a rapid *in vitro* assay (Transwell) (Falcon BD, Franklin Lakes, New Jersey), as described previously (40). Briefly, cell density was adjusted to 2×10^5 cells/ml, and 200 μl of this suspension seeded on either non-matrigel-coated (migration) or matrigel-coated (invasion) (Becton-Dickinson) upper chambers of the Transwell plate. For both assays, the pore size of the upper chamber was 8 mm. The medium in the upper chamber was serum-free DMEM, whereas the lower chamber contained DMEM supplemented with 20% FBS. After incubation for 24 h at 37 °C, cells traversing the filter from the upper to lower chamber were examined via crystal violet staining and cell counting. Experiments were performed at least three times.

Animals—Male Sprague-Dawley (S.D.) rats underwent thyroidectomy (Tx) at 6 weeks of age in accordance with previously reported methods (41). After surgery, each rat was offered drinking water containing 1% calcium lactate. At 2 weeks following surgery, rats were injected peritoneally with T_3 at 10 μg/100 g body weight or control vehicle (2.5 mM NaOH in PBS) for an additional 2 weeks. At the end of the experiment, rats were sacrificed, and the concentrations of T_3 and TSH in serum determined. The BALB/c nude mice (Jackson ImmunoResearch Laboratories, West Grove, PA) were injected subcutaneously with Huh7-PAI-1 or Huh7-control cells (each 4×10^6 cells), J7-PAI-1 or J7-control cells (each 2×10^6 cells) to determine the growth rate of the PAI-1-overexpressed cells. After 1 week of inoculation, the tumor xenografts were measured with two dimensions by caliper once per day. These nude mice were sacrificed at 4∼5 weeks after tumor inoculation. Tumor volume was calculated by the following equation: length × height × width. Another part, the severe combined immunodeficiency (SCID) mice were injected intravenously with J7-PAI-1 or J7-control cells (each 2×10^6 cells) to examine the invasive ability of PAI-1. These SCID mice were sacrificed at 4 weeks after tumor inoculation, where upon the lung and liver were removed. Similar injections were performed in nude mice or SCID mice with various T_3 conditions (Group A to C) by using J7-TR cells. The SCID mice were divided into 3 groups. Group A (euthyroid) was a control with normal drinking water. Group B (hypothyroid) was treated with 0.02% methymazole and 0.1% sodium perchlorate in the drinking water to repress T_3 synthesis (42). Additionally, Group C (hyperthyroid) was added T_3 in the drinking water (2 mg/L) (Sigma Chem. Co., St. Louis, MO) (43). The sacrifice was performed after about 1 month injection, and the T_3 concentrations were determined. Tumor volume was calculated using the following equation: length × height × width. All procedures were performed under sterile conditions in a laminar flow hood. Animal experiments were performed in accordance with United States National Institutes of Health guidelines and Chang-Gung Institutional Animal Care and Use Committee Guide for the Care and Use of Laboratory Animals.

In Vitro Neutralizing Assay—The influence of PAI-1 on T_3-mediated migration of J7-TRα1 cells was determined using a rapid *in vitro* assay (Transwell; Falcon BD). J7-TRα1 cells (5×10^4) were seeded into the non-matrigel-coated upper chamber of the transwell unit. This chamber contained serum-free DMEM whereas the lower chamber contained DMEM supplemented with 20% (v/v) FBS. J7-TRα1 cells were pretreated for 1 h with either IgG (control) or an anti-PAI-1 monoclonal antibody (catalog no. 3783; American Diagnostica, Greenwich, CT) after exposure to T_3 (10 nM, 24 h) or not (0 nM). After incubation for 24 h at 37 °C, cells traversing the filter from the upper to lower chamber were counted. All experiments were performed at least three times.

Statistical Analysis—Data are expressed as mean values ± S.E. of at least three experiments. Statistical analysis was performed using the Student's *t* test and One-way ANOVA analysis. $p < 0.05$ was considered statistically significant.

RESULTS

Identification and Quantification of the T_3-regulated Secretome Using SILAC—To investigate the TH-regulated secretome and its physiological significance, we utilized hepatocellular carcinoma (HCC) cell lines stably expressing high levels of wild-type TRα1 as a model followed by SILAC-based quantitative proteomic strategy. A schematic diagram of the experimental design for exploring the T_3-regulated secretome in HepG2-TRα1 cells is shown in Fig. 1*A*. We collected SILAC-labeled conditioned media from HepG2-TRα1 cells treated with (T_3) or without T_3 (Td) for 24 h. Prior to LC-MS/MS analysis, light and heavy proteins were concentrated and examined using Coomassie blue stain (Fig. 1*B*) and Western blot (Fig. 1*C*). Western blot analysis clearly revealed the presence of β-tubulin in the SILAC-labeled total cell extracts but not conditioned media, indicating that cell death is not the underlying reason for the presence of a high proportion of proteins in conditioned media (Fig. 1*C*). Equal amounts of heavy and light proteins were mixed and analyzed using GeLC- or 2D LC-MS/MS. In total, 1742 and 1714 unique

TABLE II

*Seventy-five candidates list. Proteins were classified using protein name in turn. *manual check*

	Swiss Prot/Uniprot		Ge-LC (E1)		2D-LC (E2)		2D-LC (E3)			Secretory pathway prediction[e]			
Candidate[a]	Accession	Protein name	Peptide[b]	T3/Td[c] ratio	Peptide[b]	T3/Td[c] ratio	Peptide[b]	T3/Td[c] ratio	Freq[d]	SignalP	SecretomeP	TMHMM	Thyroid hormone association (Ref.)
Up	P02760	AMBP	11	4.16	14	2.84	15	1.32	2/3	1	0.769	No	No
Up	P01008	ANT3	6	2.24	15	2.55	12	1.40	2/3	0.987	0.645	No	Yes (56)
Up	Q06481	APLP2	4	2.69	10	1.87	9	4.39	2/3	1	0.507	Yes	No
Up	P02652	APOA2	2	2.21	10	2.11	10	1.82	2/3	1	0.849	No	Yes (44)
Up	P06727	APOA4	13	3.27	12	3.27	13	1.50	2/3	1	0.419	No	Yes (45)
Up	Q6Q788	APOA5	4	12.94	6	3.83	7	6.02	3/3	1	0.673	No	Yes (46)
Up	P02654	APOC1			4	16.43	4	12.51	2/2	1	0.945	No	No
Up	P02655	APOC2			3	3.49	3	2.13	2/2	1	0.964	No	Yes (47)
Up	P02649	APOE	15	4.99	16	5.18	16	3.28	3/3	1	0.88	No	Yes (48)
Up	P00736	C1R	3	2.24	7	2.19	7	3.10	3/3	0.998	0.697	No	No
Up	P09871	C1S	11	2.98	9	2.70	10	2.76	3/3	1	0.73	No	No
Up	P12830	CADH1	2	3.67	4	4.76	4	1.71	2/3	0.999	0.179	Yes	Yes (49)
Up	O15467	CCL16			3	3.74	2	7.25	2/2	0.999	0.921	No	No
Up	P08571	CD14	3	42.20	8	34.84	9	51.47	3/3	1	0.674	No	No
Up	P11597	CEIP	2	4.25	7	10.52	7	14.00	3/3	0.999	0.73	No	Yes (50)
Up	P36222	CH3L1	7	3.59	7	3.40	10	2.18	3/3	0.998	0.645	No	No
Up	Q9BWS9	CHID1	2	2.45	9	2.62	10	4.58	3/3	1	0.733	No	No
Up	P01024	CO3	71	2.27	89	2.29	81	1.99	2/3	1	0.618	No	Yes (13)
Up	P39060	COIA1			8	7.60	10	12.97	2/2	0.998	0.166	No	Yes (51)
Up	Q9NZV1	CRIM1	5	4.00	4	3.08	4	2.22	3/3	0.995	0.521	Yes	No
Up	Q9H2A7	CXL16			2	3.52	3	2.59	2/2	0.941	0.179	Yes	No
Up	Q9UBS4	DJB11	5	11.09	8	10.46	8	21.26	3/3	0.982	0.707	Yes	No
Up	Q13217	DNJC3			3	2.15	2	11.98	2/2	0.889	0.38	No	No
Up	Q9Y6C2	EMIL1			8	3.12	12	4.76	2/2	1	0.239	No	No
Up	Q13822	ENPP2	10	4.83	24	4.82	23	4.36	3/3	0.89	0.488	Yes	Yes (52)
Up	P62495	ERF1	4	1.73	5	2.00	3	7.14	2/3	0	0.444	No	No
Up	P02671	FIBA	10	2.21	26	6.56	15	1.85	2/3	0.999	0.397	No	Yes (53)
Up	P02675	FIBB	6	2.67	24	3.09	12	1.28	2/3	0.999	0.534	No	Yes (53)
Up	P02679	FIBG	18	2.48	19	2.85	18	2.18	3/3	0.932	0.696	Yes	Yes (13)
Up	P02751	FINC	39	2.23	62	2.92	65	6.91	3/3	0.997	0.369	No	Yes (13)
Up	O95633	FSTL3			2	3.78	3	2.53	2/2	0.995	0.9	No	Yes (54)
Up	P09958	FURIN			5	7.61	6	6.36	2/2	0.982	0.388	Yes	Yes (16)
Up	Q99988	GDFI5	7	12.37	16	12.44	16	21.12	3/3	0.996	0.882	No	No
Up	P06396	GELS			14	3.11	13	3.05	2/2	1	0.553	No	No
Up	P35052	GPC1			5	3.46	5	3.92	2/2	1	0.33	No	No
Up	Q16270	IBP7	2	5	5	1.65	5	4.98	2/3	0.998	0.536	No	No
Up	P30740	ILEU	5	2.27	8	2.17	4	1.19	2/3	0.015	0.516	No	No
Up	P05154	IPSP	9	1.91	10	6.31	6	2.00	3/3	1	0.838	No	No
Up	P19823	ITIH2	23	2.22	45	2.29	39	4.03	3/3	1	0.509	No	No
Up	P01042	KNG1			3	4.05	3	2.87	2/2	0.996	0.489	No	No
Up	P55268	LAMB2	3	2.36	4	2.72	6	1.68	2/3	0.877	0.261	No	No
Up	P01130	LDLR	3	3.31	9	3.24	8	1.92	2/3	0.999	0.475	Yes	Yes (55)
Up	P48740	MASP1	4	9.39	8	3.43	8	2.18	3/3	1	0.705	No	No
Up	Q86UD1	OAF			4	3.78	3	4.58	2/2	1	0.938	No	No
Up	P05121	PAI1	7	4.66	19	4.53	16	4.71	3/3	0.999	0.644	No	Yes (59)
Up	Q15084	PDIA6	2	2.13	9	1.82	7	4.06	2/3	0.999	0.711	No	No
Up	P20142	PEPC			2	3.97	2	2.07	2/2	0.999	0.866	No	No
Up	Q96NZ9	PRAP1			5	4.84	8	4.20	2/2	1	0.822	No	No
Up	P10586	PTPRF	5	3.27	7	3.73	14	3.43	3/3	0.998	0.419	Yes	No
Up	P31431	SDC4	2	13.20	4	6.76	3	7.61	3/3	1	0.557	Yes	No
Up	Q13214	SEM3B			7	2.42	10	3.43	2/2	1	0.343	Yes	No
Up	Q13275	SEM3F			3	3.19	3	2.96	2/2	1	0.5	No	No
Up	O75326	SEM7A	5	5.20	8	5.70	6	2.66	3/3	0.999	0.484	No	No
Up	P04278	SHBG			5	3.48	6	2.06	2/2	1	0.708	No	No
Up	P50453	SPB9	3	3.14	4	3.29	2	1.91	2/3	0.016	0.559	No	No
Up	Q9BUD6	SPON2			2	10.47	2	11.03	2/2	0.999	0.766	No	Yes (37)
Up	Q92563	TICN2	7	9.33	16	4.99	18	7.22	3/3	1	0.232	No	No
Up	P16035	TIMP2	4	3.58	5	4.22	2	3.50	3/3	1	0.854	No	No
Up	Q8WUA8	TSK	2	14.48	2	5.32	3	25.89	3/3	1	0.724	No	No
Up	P02774	VTDB	2	3.42	10	3.10	5	0.59	2/3	1	0.434	No	No
Up	Q6PCB0	VWA1			6	3.07	3	2.75	2/2	1	0.517	No	Yes (57)
*Up	Q03405	UPAR			2	7.80			1/1		0.737	No	No
*Up	Q9GZN4	BSSP4	3				3	3.25	1/1	0.989	0.744	No	No
Down	P19022	CADH2	6	0.40	9	0.37	7	0.56	2/3	0.999	0.203	Yes	No
Down	P10909	CLUS	8	0.48	10	0.58	10	0.5	2/3	1	0.826	No	Yes (13)
Down	P15924	DESP	8	0.03	4	0.5	3	1.71	2/3	0	0.183	No	No
Down	O94907	DKK1	2	0.20	6	0.31			2/2	0.997	0.952	No	No
Down	P02794	FRIH			4	0.49	3	0.38	2/2	0	0.621	No	Yes (58)
Down	P38159	HNRPG	3	0.32	4	0.41	3	3.53	2/3	0	0.276	No	No

TABLE II—*continued*

Candidate[a]	Swiss Prot/Uniprot		Ge-LC (E1)		2D-LC (E2)		2D-LC (E3)			Secretory pathway prediction[e]			
	Accession	Protein name	Peptide[b]	T3/Td[c] ratio	Peptide[b]	T3/Td[c] ratio	Peptide[b]	T3/Td[c] ratio	Freq[d]	SignalP	SecretomeP	TMHMM	Thyroid hormone association (Ref.)
Down	Q86YZ3	HORN	7	0.03	3	0.01	3	25.1	2/3	0.019	0.087	No	No
Down	Q8WUJ3	K1199	8	0.14	18	0.18	12	0.16	3/3	0.993	0.42	No	No
Down	P14923	PLAK	6	0.14	6	0.4			2/2	0	0.475	No	No
Down	P06737	PYGL	5	0.39	10	0.5	10	0.72	2/3	0	0.381	No	No
Down	O15240	VGF			3	0.42	3	0.27	2/2	1	0.315	No	No
*No-change	Q16658	FSCN1	4	0.95	4	0.95	3	0.87	3/3	0.001	0.385	No	No

[a] Up-regulated, down-regulated and non-changed by T_3.
[b] Peptide, the number of identified peptides.
[c] Fold change in target protein expression in T_3 treatment (T_3) or not (Td) cells.
[d] Freq, frequency of target up, down-regulated and non-changed proteins in detectable samples.
[e] Proteins predicted secretory pathway using singalP, secretomeP and TMHMM software.

TABLE III
Biological network of 72 expressed proteins by MetaCore software analysis

GeneGo map	p-Value	Features (Proteins)
1. Blood coagulation_Blood coagulation	4.434e-13	Up: PAI-1, FINC, FIBG, KNG1, ANT3, IPSP5
2. Immune response_Classical complement	1.452e-12	Up: CO3, C1R, C1S Down: CLUS
3. Immune response_Lectin induced complement pathway	4.727e-11	Up: CO3, MASP1 Down: CLUS
4. Cell adhesion_Cadherin-mediated cell adhesion	6.024e-6	Up: PTPRF, CADH1 Down: CADH2, PLAK
5. Development_TGF-beta-dependent induced of EMT via SMADs	2.046e-5	Up: PAI-1, CADH1, FINC Down: CADH2

proteins were identified and quantified, respectively, in three independent experiments, the data from which are shown in Fig. 1*D*. Of these proteins, 1205 identified and 1176 quantified proteins were consistently present in at least two of the three tests (Fig. 1*D*). The details of peptide and protein identification and quantification are shown in supplementary Tables S1 and S2, respectively.

To elucidate the potential secretion mechanisms of the identified proteins, different bioinformatics programs, including SignalP, SecretomeP, and TMHMM, were employed. The predicted secretion pathways of proteins identified in the three experiments (E1+E2+E3) are summarized in Table I. Among the 1742 proteins, SignalP predicted that 399 were released via the classical secretion pathway (SignalP probability $\geq$0.90), the SecretomeP program predicted that another 484 were secreted via the nonclassical secretion pathway (SignalP probability $<$0.90 and SecretomeP score $\geq$0.50), and the TMHMM program estimated that 26 others were not secreted via either the classical or non-classical secretion pathways. Collectively, our data suggest that 52.2% (909 of 1742) of the identified proteins are potentially released into extracellular space via different pathways.

Validation and Pathway Analysis of Protein Candidates—Using twofold change as the criterion for selection of T_3-regulated candidates, 50, 83, and 232 up-regulated as well as 20, 41, and 59 down-regulated proteins in T_3-treated cells were identified in the E1, E2, and E3 experiments, respectively (Fig. 1*E*). Among these, 61 and 11 proteins that were consistently up-regulated and down-regulated, respectively, in two (or more) of the three experiments were selected as T_3-regulated candidates (Table II). Twenty-three of the 72 candidates (31.9%) have been previously determined as T_3-associated proteins (13, 16, 37, 44–59), and the remaining proteins detected for the first time in this study.

To explore the statistically significant biological networks regulated by T_3, the 72 candidates were analyzed using the GeneGo pathway map tool of MetaCore™ (60). The analysis revealed five significant pathways ($p < 0.0001$) with at least three participating candidates (Table III), including blood coagulation, classical and lectin-induced complement pathways, cadherin-mediated cell adhesion, and the TGF-β-dependent development network. Seven of 15 candidates involved in these pathways have previously been reported as T_3-regulated target genes, specifically, ANT3, CADH1, CLUS, CO3, FIBG, FINC, and PAI-1 (Tables II and III).

Ten differentially expressed candidates (including 8 increases, 1 decrease and 1 no change) with available antibodies were selected for further Western blot analyses, with a view to validate the quantitative proteomics results. As shown in Fig. 2, all proteins were regulated by T_3 in a dose-dependent manner. Western blotting data were consistent with the MS-based quantitative results. The MS spectra of the representative peptides of proteins are displayed in Fig. 2. For example, fascin1 was not altered following T_3 treatment and thus taken as a reference for the other T_3-regulated targets. Notably, the levels of fibrinogen (FIBG), fibronectin (FINC),

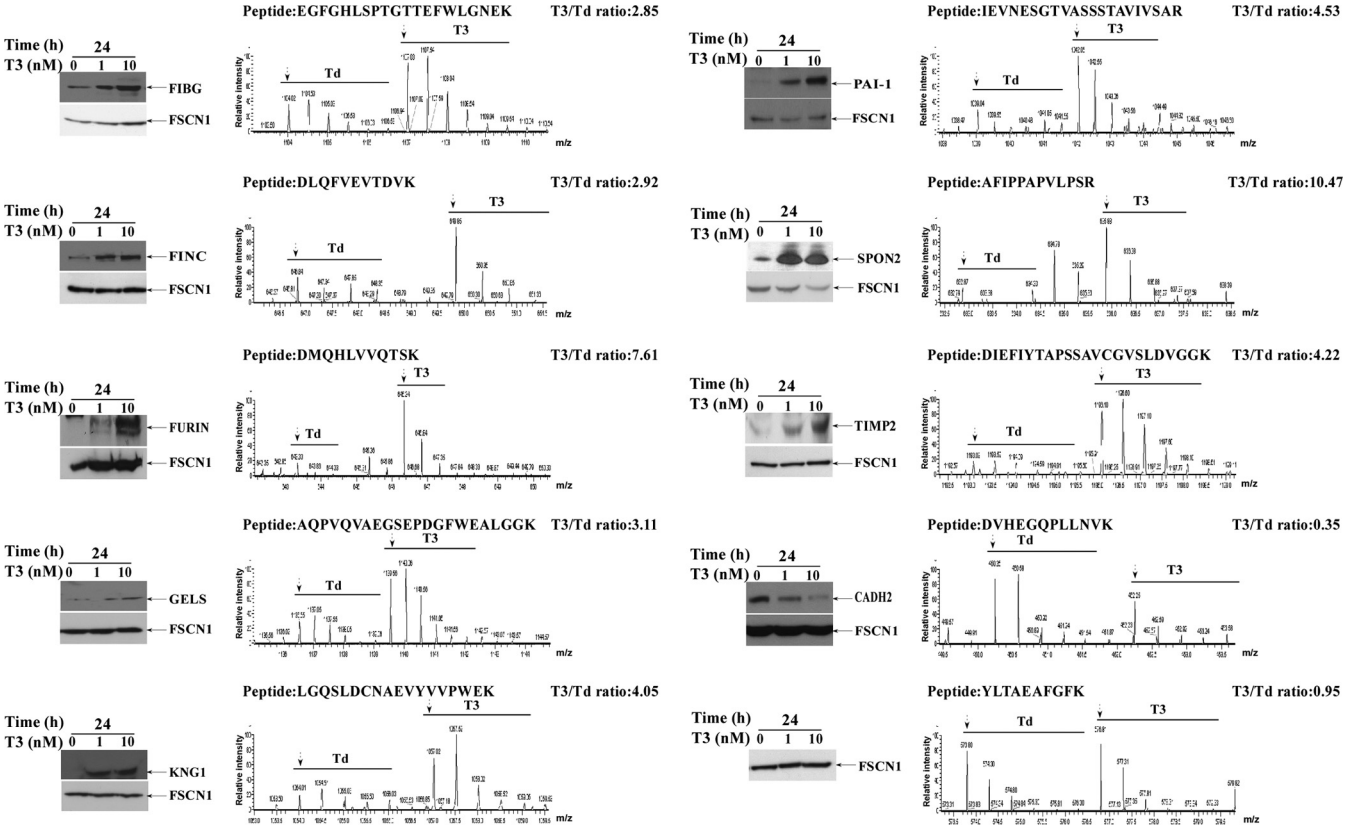

FIG. 2. **Validation of identified proteins.** Conditioned media of HepG2-TRα1 cells treated with different concentrations of T_3 (0, 1, 10 nM) at 24 h were electrophoresed using 12% SDS-PAGE, followed by Western blot analysis. The MS spectrum, identified peptide sequence, and quantified T_3/Td ratio (arrow, first peak of spectrum; T_3, 10 nM; Td, T_3-depleted) are presented.

furin (FURIN), gelsolin (GELS), kininogen-1 (KNG1), plasminogen activator inhibitor-1 (PAI-1), spondin-2 (SPON2), and metalloproteinase inhibitor-2 (TIMP2) were increased, and cadherin-2 (CADH2) decreased in conditioned media after T_3 treatment. Based on the above data, we propose that T_3 is potentially involved in both blood coagulation and progression of the epithelial-mesenchymal transition via regulation of PAI-1 (Table III), which is known to participate in these biological pathways (see the REACT_604 data).

Previously, we reported that T_3 plays an important role in blood coagulation by stimulating the expression of fibrinogen and a few blood clotting factors. PAI-1 inhibits the serine proteases tissue-type plasminogen activator (tPA) and urokinase (u)PA/urokinase, and hence inhibits fibrinolysis. Additionally, PAI-1 is particularly associated with the process of metastasis, poor prognosis and high mortality (26). Earlier, Biz *et al.* showed that thyroid hormones increase the level of PAI-1 mRNA expression in 3T3-L1 adipocytes (59). This finding links T_3 and PAI-1 expression. In view of these findings, PAI-1 was selected for further study.

Effects of T_3 Treatment on PAI-1 mRNA and Protein Expression—Four HepG2 cell lines, including HepG2-TRα1#1, HepG2-TRα1#2, HepG2-TRβ1, and HepG2-neo expressing various levels of TR, were established (Fig. 3*A*). Regulation of PAI-1 by different concentrations of T_3 at different time-points was investigated. Notably, PAI-1 expression was stimulated by T_3 in the HepG2-TRα1#1, HepG2-TRα1#2, and HepG2-TRβ1 cell lines, both at the mRNA (up to 17×, Fig. 3*B*) and protein levels (up to ~20×, Fig. 3*C*). However, T_3 had marginal or no effect on PAI-1 expression in HepG2-neo cells (Figs. 3*B*, 3*C*). The data suggest the PAI-1 regulation by T_3 is TR-dependent. We selected three other HCC cell lines (Huh7, J7, and Mahlavu) expressing detectable endogenous TR. Similarly, PAI-1 was activated after treatment with 0, 1, and 10 nM T_3 at 12, 24, and 48 h in parental Huh7 hepatoma cell lines (Fig. 3*C*, data not shown). Thus, T_3 appears to regulate PAI-1 in both HepG2 isogenic cell lines and those with detectable endogenous TR.

To further determine the *in vivo* response of PAI-1 to T_3, two groups of 6 week-old male S.D. rats ($n = 6$ in each group) were surgically thyroidectomized. Subsequently, one of the thyroidectomized groups (Tx), used as the sham-operated control (sham), did not receive the T_3 injection, whereas the other group (Tx+T_3) was injected with T_3 daily for 2 weeks. After 2 weeks, rats were sacrificed, livers were removed and serum from each group were collected to examine the concentrations of T_3 and TSH, respectively (16). The T_3-treated group (Tx+T_3) displayed enhanced *PAI-1* mRNA and protein

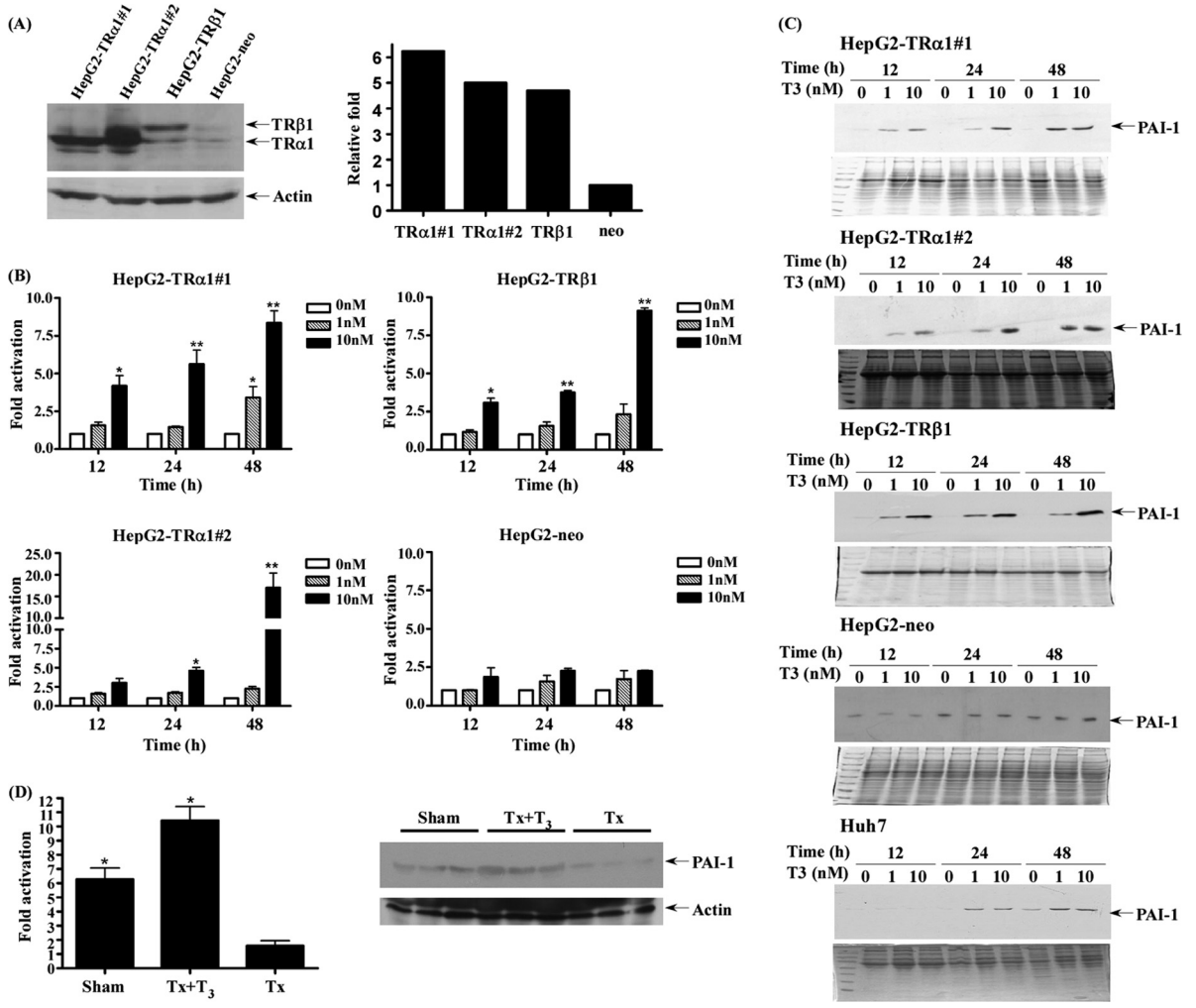

FIG. 3. **T_3-regulated PAI-1 expression in HepG2 cells.** *A*, Expression of TR was determined via Western blotting in cell extracts of three HepG2-TR stable lines and HepG2-neo cells. HepG2 cells were transfected with TRα1 or TRβ1, as described under "Experimental Procedures." The positions of 47 kDa TRα1 and 55 kDa TRβ1 are indicated. TR bands are quantified in the right panel. PAI-1 expression was determined in the three HepG2-TR stable lines and HepG2-neo cells at 12–48h in the absence or presence of 1 and 10 nM T_3 using (*B*) Q-PCR and (*C*) Western blotting. *D*, PAI-1 expression was induced by T_3 and determined using Q-PCR and Western blotting in rat liver (sham, Tx, Tx+T_3), as described under "Experimental Procedures." Values are shown as fold induction of PAI-1mRNA relative to 0 nM T_3 at each time point or Tx. Differences were analyzed using the One-way ANOVA analysis, $^{**}p < 0.01$; $^{*}p < 0.05$.

expression, compared with the Tx group (Fig. 3*D*). These measurement results support the regulation of PAI-1 expression by thyroid hormones.

T_3 Induces PAI-1 Expression at the Transcription Level—To further clarify whether T_3 affects *PAI-1* regulation at the transcriptional level, the reporter assay was performed to locate the thyroid hormone response element (TRE). The *PAI-1* 5′flanking region encompassing nucleotides –2261/+1203 (relative to the transcription initiation site) with three predicted putative TREs (Fig. 4*A*) was cloned and inserted upstream of the luciferase reporter gene in pGL2-luc (Construct p1) and pA3TK-luc (containing a minimum thymidine kinase promoter) vectors (Construct p4). Moreover, serial deletion mutants were constructed (Fig. 4*A*, *left*). The transcriptional activities of the *PAI-1* promoter fragments are illustrated in Fig. 4*A*, *right*. The luciferase activity of the –2261/+1203 construct (p2) was increased 6.7-fold in the presence of 10 nM T_3 in HepG2-TRα1 cells, compared with the activity of the pGL2-luc vector. Four truncated fragments were further cloned and transfected into HepG2-TRα1 cells, specifically, –169/+1203 (p3), –2261/–1733 (p5), –1820/–1200 (p6), and –780/–169 (p7) constructs. Among these, only the –780/–169 (p7) construct was activated about eightfold after T_3 treatment. Subsequently, we divided the –780/–169 (p7) construct into –760/–400 (p8) and –520/–130 (p9) fragments, and showed that only the latter construct (–520/–130) was activated (~7.5-fold) by T_3. The –520/–130 (p9) fragment was predicted to contain the three putative TREs. This fragment was further divided into three regions, –379/–277 (p10), –219/–140 (p11), and –520/–360 (p12). Among these, only the –379/–277 (p10) con-

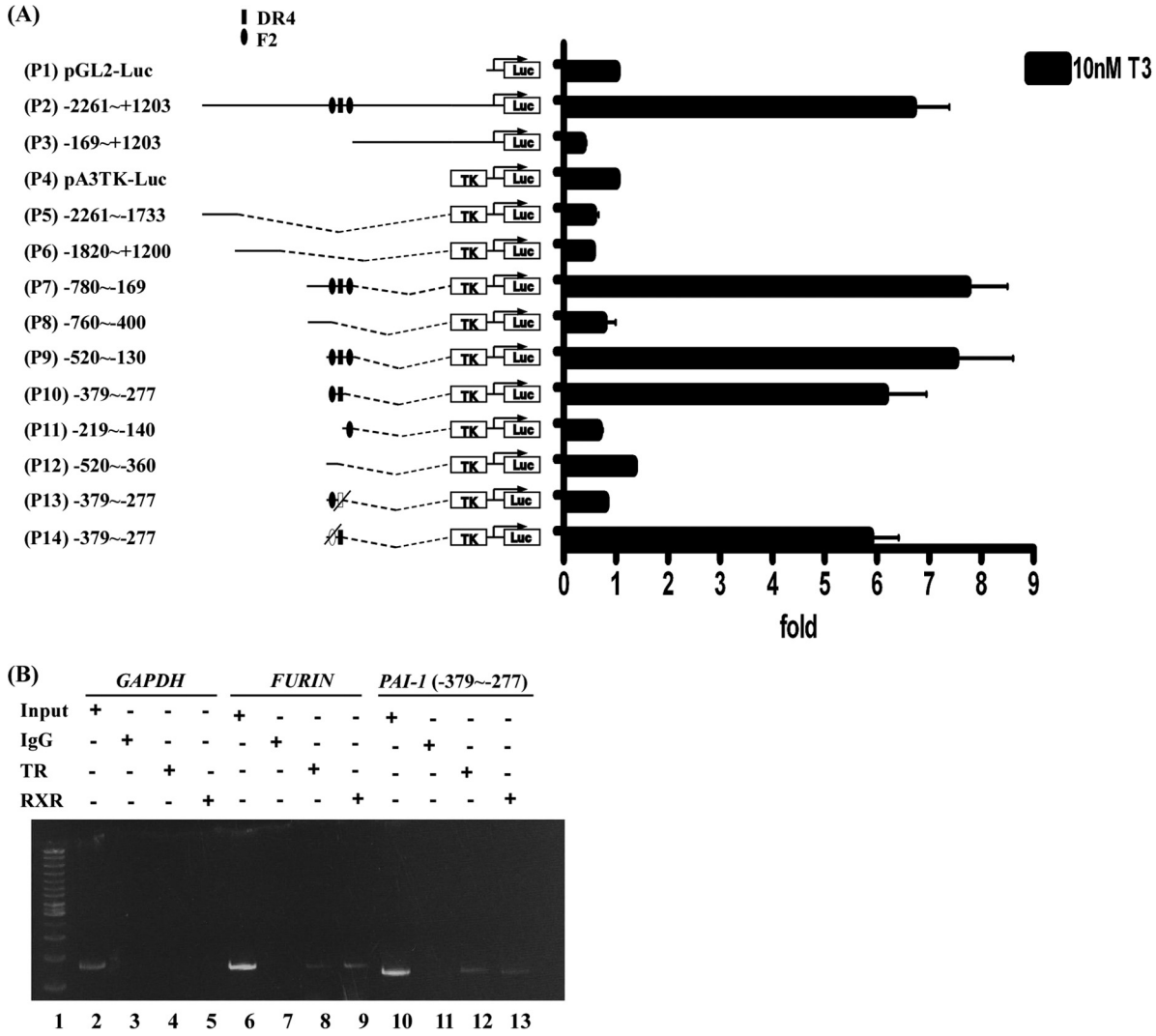

FIG. 4. **Regulation of *PAI-1* expression by T_3 at the transcriptional level.** *A*, HepG2-TRα1 cells were transfected with luciferase reporter plasmid driven by the *PAI-1* 5′-flanking region (positions –2261 to +1203 containing three putative TRE sites) with or without a pA3TK-luc. Promoter activities were calculated, relative to 0 nM T_3 (+T_3/-T_3), and further normalized to the pA3TK-luc control as well as β-galactosidase activities (T_3-induced changes were normalized to that of β-gal). Columns, mean values obtained from at least three independent experiments performed in triplicate; bars, S.E. Cells were incubated for 24 h in the presence or absence of T_3 (10 nM) before harvesting to determine luciferase activity. Deletions and mutations in the *PAI-1* 5′-flanking region were also generated in pA3TK-luc vector, and the resulting constructs transfected into cells. *B*, ChIP assay demonstrating that TR is recruited to the *PAI-1* 5′-flanking region, together with RXR. Two sets of primers for *PAI-1* TRE, positive control TRE (*FURIN*) and negative control (*GAPDH*) were prepared. ChIP assay data were evaluated with PCR and gel electrophoresis. Representative results are shown.

struct containing two putative TREs was activated about sixfold by T_3 in HepG2-TRα1 cells. The two TREs in the –379/–277 (p10) fragment were sequentially mutated to yield p13 and p14 constructs. After mutation of putative TRE (F2), luciferase activity of the p14 construct was still stimulated by about sixfold by T_3 in HepG2-TRα1 cells. Conversely, after mutation of putative TRE (DR4), luciferase activity of the p13 construct was completely abolished (Fig. 4*A*, *right*). These data strongly suggest that T_3 regulates *PAI-1* expression at the transcriptional level, and the putative TRE site exists between positions –379/–277 (p10) encompassing a DR4-like sequence between positions –327~–312 (AGGTCA AGGG AGGTTC).

TR and RXR Proteins Form a Complex with TRE (−327~−312) Located in the PAI-1 Promoter—To further determine whether *PAI-1* TRE (DR4) is directly targeted by TR proteins, the ChIP assay was performed. TR proteins clearly associated with the TRE region of the *PAI-1* promoter *in vivo* (Fig. 4*B*). TRα1 and RXRα were clearly recruited to the TRE-binding site (Fig. 4*B*, lanes 12 and 13), whereas control IgG produced only background levels (lane 11). The positive control (human *FURIN* gene containing TRE) showed detectable bands with antibodies against TRs or RXRα (lanes 8–9). However, no bands were detected using a primer set for the negative control (human *GAPDH* gene, lanes 3–5). Data from the ChIP

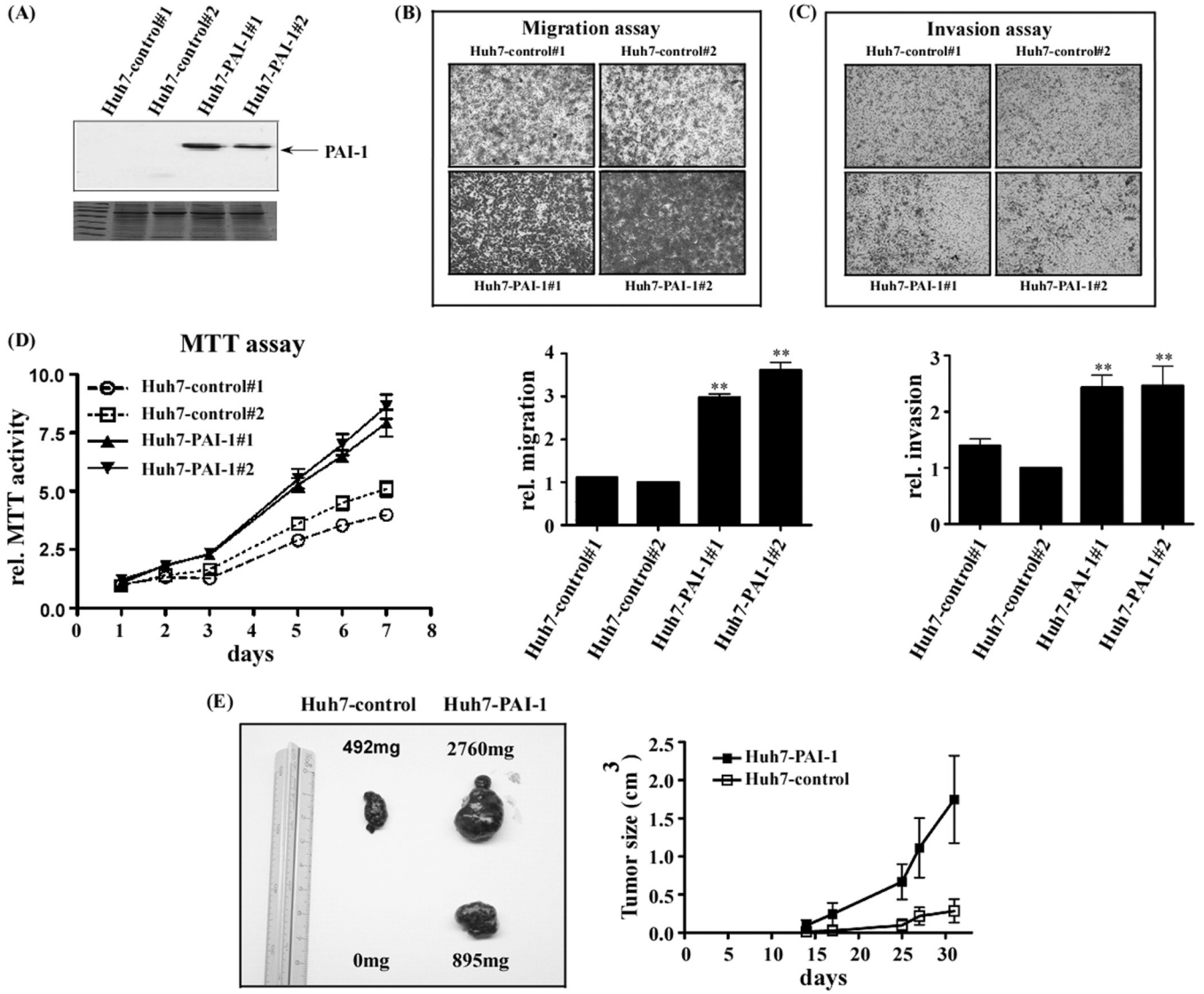

FIG. 5. **Functional assay of PAI-1 in hepatoma cells.** The pcDNA3.0-*PAI-1* or pcDNA3.0 construct was transfected into Huh7 cells to establish stable Huh7-PAI-1 or Huh7-control lines. Expression of PAI-1 was detected in PAI-1-overexpressing clones (#1, #2) and controls (control#1, #2) with Western blotting (*A*). *B*, Migration and (*C*) invasion abilities were analyzed through a Transwell assay in two PAI-1 over-expressing and two control cell lines. The stable lines (5×10^4) were added to the upper chamber of Transwell units and incubated for 24 h. The number of cells traversing the filter to the lower chamber was determined and expressed as the total number of cells to provide an index of migration and invasion activity. Transwell filters were stained with crystal violet in the *upper* panel, and migration and invasion ability quantified in the *lower* panel. Values are shown as fold increase of Huh7-PAI relative to Huh7-control. Differences were analyzed using the One-way ANOVA analysis, $^{**}p < 0.01$. (D) Proliferation ability was analyzed with the MTT assay, as described under "Experimental Procedures." Cell growth rates were determined based on absorption at 570 nm/650 nm up to 7 days. *E*, Nude mice were injected subcutaneously with Huh7-control (*left*) and Huh7-PAI-1 (*right*). Assays were performed 5 weeks after inoculation of tumor cells. The image showed two reprehensive tumor volumes in nude mice (total $n = 3$) after 5 weeks. The statistics graph indicates that tumor size increased with time, both in control cells and those overexpressing PAI-1 up to 5 weeks.

assay thus demonstrate that the TRα1 and RXRα complexes bind to the *PAI-1* promoter.

PAI-1 is Associated with Cell Motility and Proliferation In Vitro or In Vivo—To determine the function of PAI-1, PAI-I overexpressing (Fig. 5*A*, Huh7-PAI-1 #1 and #2) or control cell lines (Fig. 5*A*, Huh7-control #1 and #2) were established. Notably, cell lines with overexpression of PAI-1 (Huh7-PAI-1 #1 and #2) displayed significantly increased (~two- to threefold) migration and invasion, compared with control cells (Huh7-control #1 and #2) (Figs. 5*B*, 5*C*). Images of cells migrating through the upper chamber stained with crystal violet are presented in Figs. 5*B* and 5*C*. Fig. 5*D* shows the proliferation rates of the two cell lines stably overexpressing PAI-1 (Huh7-PAI-1 #1 and #2), which were higher than those of the two control cell lines (Huh7-control #1 and #2). The expression level of PAI-1 in Huh7 cells

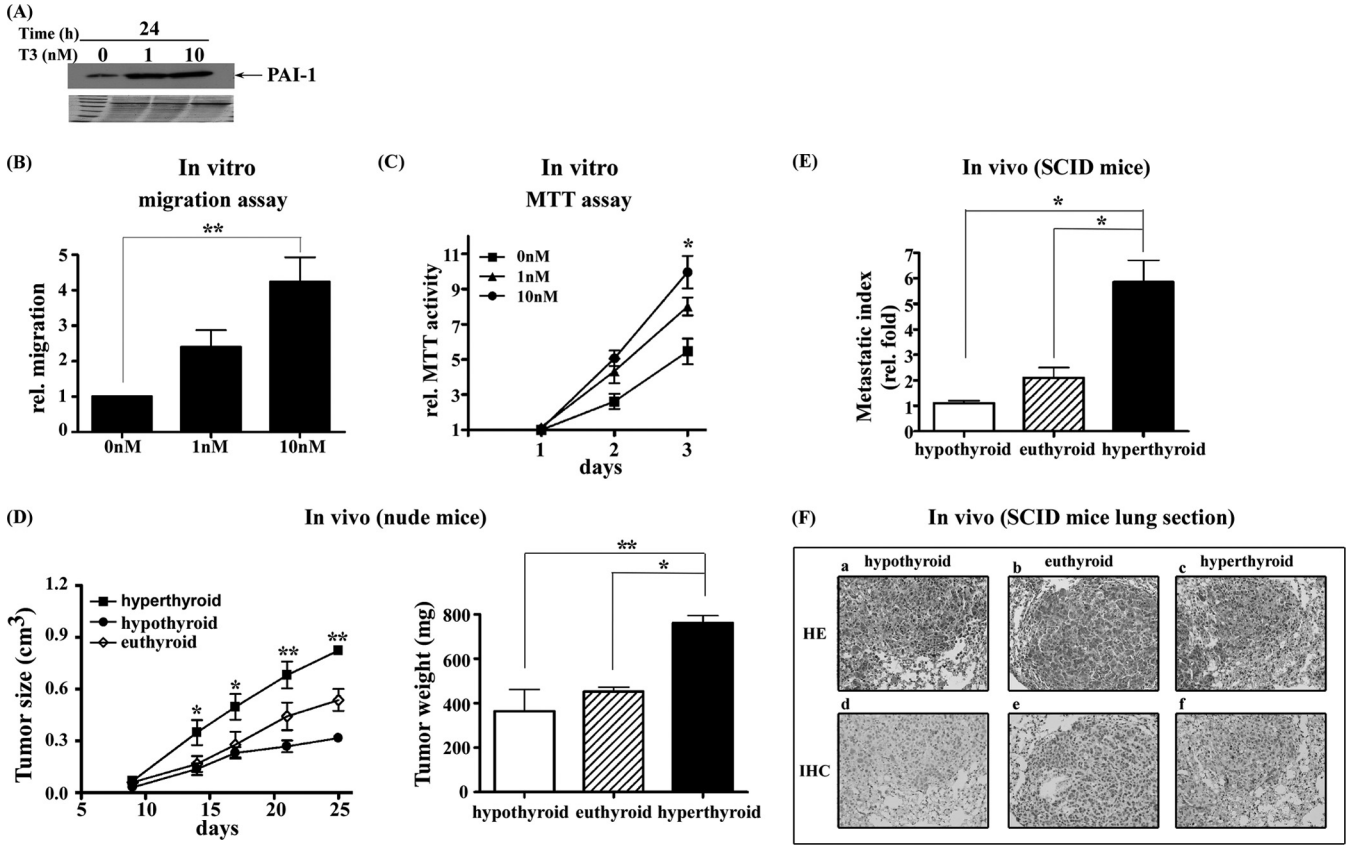

FIG. 6. **T3 increased J7-TRα1 cell migration and proliferation both *in vitro* and *in vivo*.** PAI-1 expression was determined in the (*A*) J7-TRα1 cells treated with or without 1 or 10 nM T_3 for 24h using Western blotting. *In vitro* (*B*) migration and (*C*) proliferation were analyzed through a Transwell assay or MTT assay in J7-TRα1 cells in the absence or presence of 1 or 10 nM T_3, as described under "Experimental Procedures." *D*, The nude mice injected subcutaneously with J7-TRα1 cells that were divided into hyperthyroid, euthyroid and hypothyroid groups ($n = 6$ per group). The tumor sizes and weights of three groups were measured up to 25 days after inoculation of tumor cells. *E*, The metastasis index (fold, density of tumor numbers in per cm^2 area) in the lung of J7-TRα1 cells (hyperthyroid, euthyroid and hypothyroid) are shown. The (*F*) tumor foci and PAI-1 expression were displayed by H&E staining and IHC, respectively. The tumor foci cover almost all areas seen in (*F*). Values are shown as fold induction relative to 0 nM T_3 or hypothyroid. Differences were analyzed using the One-way ANOVA analysis, $^{**}p < 0.01$; $^{*}p < 0.05$.

induced with 10 nM T_3 for 24 h was about 40% that of Huh7-PAI-1 cells (data not shown).

To investigate whether the effects of PAI-1 in vitro could be applied *in vivo*, nude mice were employed. We established a xenograft of stable Huh7-PAI-1 cells in BALB/c nude mice. Nude mice were subcutaneously injected with Huh7-PAI-1 or Huh7-control (Fig 5*E*), and tumor sizes measured from two to five weeks after injection. Tumor volume and weight are shown in Fig. 5*E left* (*right*: Huh7-PAI-1, *left*: Huh7-control). Additionally, tumor sizes from the two groups (Huh7-PAI-1 and Huh7-control) of mice are illustrated in Fig. 5*E right*. On average, tumors sizes of mice injected with Huh7-PAI-1 cells were two- to fivefold larger than those of control mice.

PAI-1 May Contribute to T_3-mediated Phenotypes—To explore the function of PAI-1 induced by T_3, J7-TRα1 cells were established (Fig. 6*A*). Notably, PAI-1 was induced about threefold by various doses of T_3 (Fig. 6*A*), and such cells showed significant increases (~fourfold) in migration (Fig. 6*B*) and proliferation (twofold; Fig. 6*C*), compared with control values (obtained from cells not exposed to T_3).

To investigate whether the *in vitro* effect of T_3 was evident *in vivo*, nude and SCID mice were injected with J7-TRα1 cells. The animals were subjected to hyperthyroid, euthyroid, and hypothyroid conditions after injection. In the *in vivo* proliferation assay, tumors in hyperthyroid nude mice were larger (Fig. 6*D*, *left*) and heavier (Fig. 6*D*, *right*) than was the case with the other two groups (Fig. 6*D*). Further, the hyperthyroid group of SCID mice, injected with J7-TRα1 cells, displayed more lung foci, a higher metastatic index (Fig. 6*E*), and a more elevated level of PAI-1 expression than did the other groups, as shown by hematoxylin and eosin staining (H&E) (Fig. 6*F*; a, b, c) and immunohistochemistry (IHC) (Fig. 6*F*, d, e, f), respectively.

Additionally, stable J7-PAI-1 lines were established. Two stable PAI-1 clones (J7-PAI-1 #1 and #2) expressed PAI-1 at levels at least seven- to eightfold higher than those of the two control lines (J7-control #1 and #2) (Fig. 7*A*). Notably, two cell

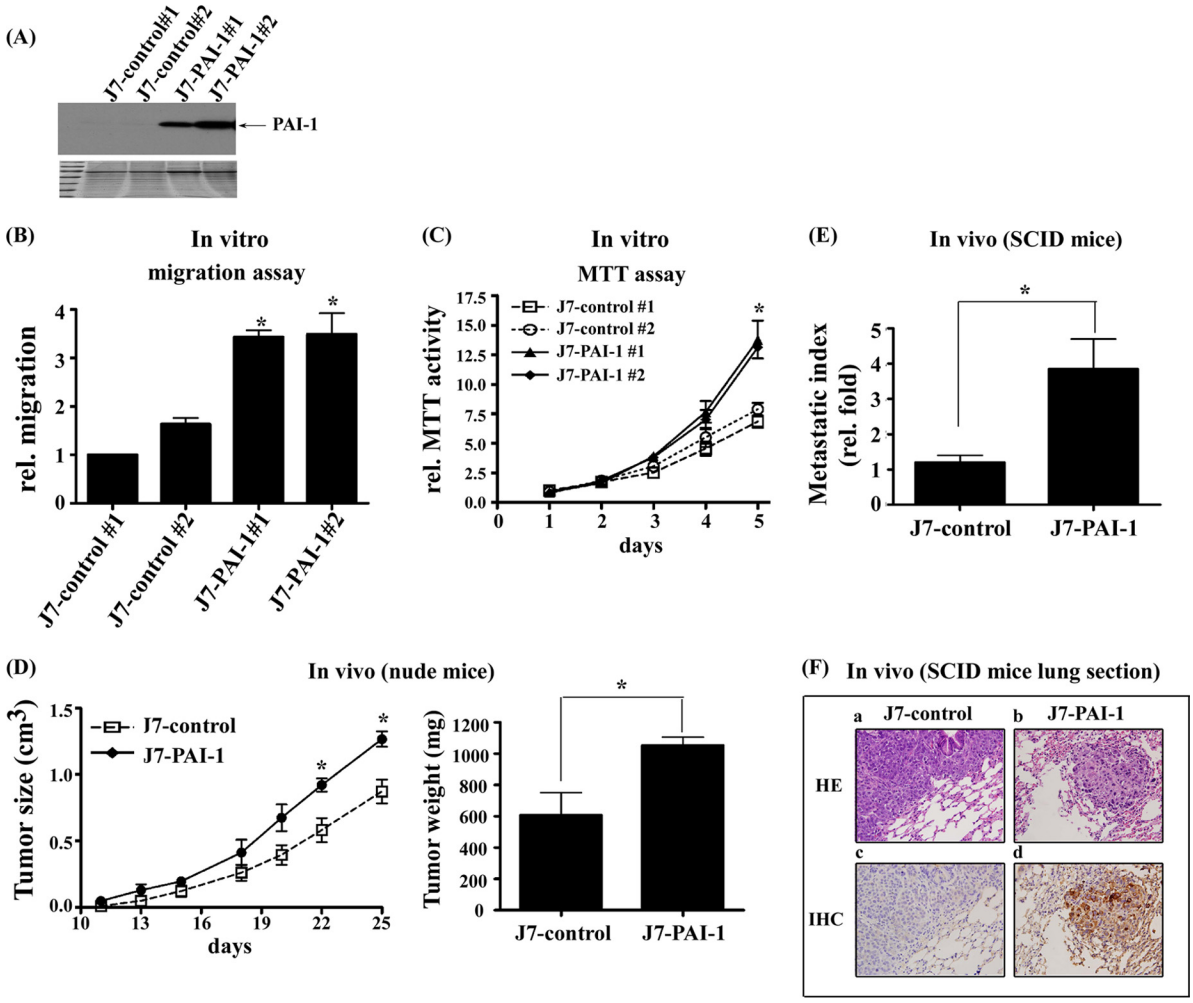

FIG. 7. **PAI-1 increased cell migration and proliferation in J7 cells both *in vitro* and *in vivo*.** PAI-1 expression was determined in (*A*) J7-PAI-1 and control stable lines using Western blotting. *In vitro* (*B*) migration and (*C*) proliferation were analyzed through a Transwell assay and MTT assay of two PAI-1 over-expressing and two control cell lines, as described under "Experimental Procedures." *D*, The nude mice injected subcutaneously with J7-control and J7-PAI-1 cells. The tumor sizes (*left*) and weights (*right*) were measured up to 25 days after inoculation of tumor cells. The metastasis index (fold, density of tumor numbers in per cm^2 area) in lung of (*E*) J7-PAI-1 and J7-control cells are shown. The (*F*) tumor foci and PAI-1 expression of J7-control and J7-PAI-1 cells were displayed by H&E staining or IHC, respectively. The tumor foci cover almost all areas seen in (*F*). Values are shown as fold increase relative to J7-control. Differences were analyzed using the Student's *t* test or One-way ANOVA analysis, $^*p < 0.05$.

lines showing elevated PAI-1 expression (J7-PAI-1) exhibited increased migration (Fig. 7*B*) and proliferation (Fig. 7*C*) *in vitro*. To investigate whether the effects of PAI-1 *in vitro* could be observed *in vivo*, nude and SCID mice were employed. In nude mice, tumors overexpressing PAI-1 were clearly larger (Fig. 7*D*, *left*) and heavier (Fig. 7*D*, *right*) than were tumors containing J7 control cells (Fig. 7*D*). Similarly, in SCID mice, J7-PAI-1 cells formed higher numbers of lung foci and had a higher metastatic index (Fig. 7*E*) compared with control cells, as shown by H&E staining (Fig. 7*F*; a, b) and IHC (Fig. 7*F*; c, d), respectively. The PAI-1 expression level in J7-TRα1 cells induced with 10 nM T_3 for 24 h was about 90% that of J7-PAI-1 cells (data not shown). Regardless of whether the PAI-1 expression was inducible (T_3-induced J7-TRα1) or constitutive (J7-PAI-1), cellular migration and proliferation were increased in the two cell lines both *in vitro* and *in vivo* (Figs. 6 and 7).

Previously, we showed that cathepsin H (CATH) expression was also directly regulated by T_3 in human hepatoma cell lines and that CATH enhanced the metastatic potential of hepatoma cells by increasing the activities of MMP-2 (61). Therefore, we sought to understand whether MMP2 or MMP9 was a downstream effector of PAI-1 as both MMPs share the same substrate. MMPs are zinc- and calcium-dependent endopeptidases involved in proteolytic processing (62). The activities of MMP2 and MMP9 were determined with the gelatin zymography assay. Both pro-MMP2 (72 kDa) and active MMP2 (67 kDa) activities were increased in PAI-1-overexpressing stable lines (Huh7-PAI-1 #1 and #2), but not in control cells (Huh7-control #1 and #2). In contrast, pro-MMP9 and

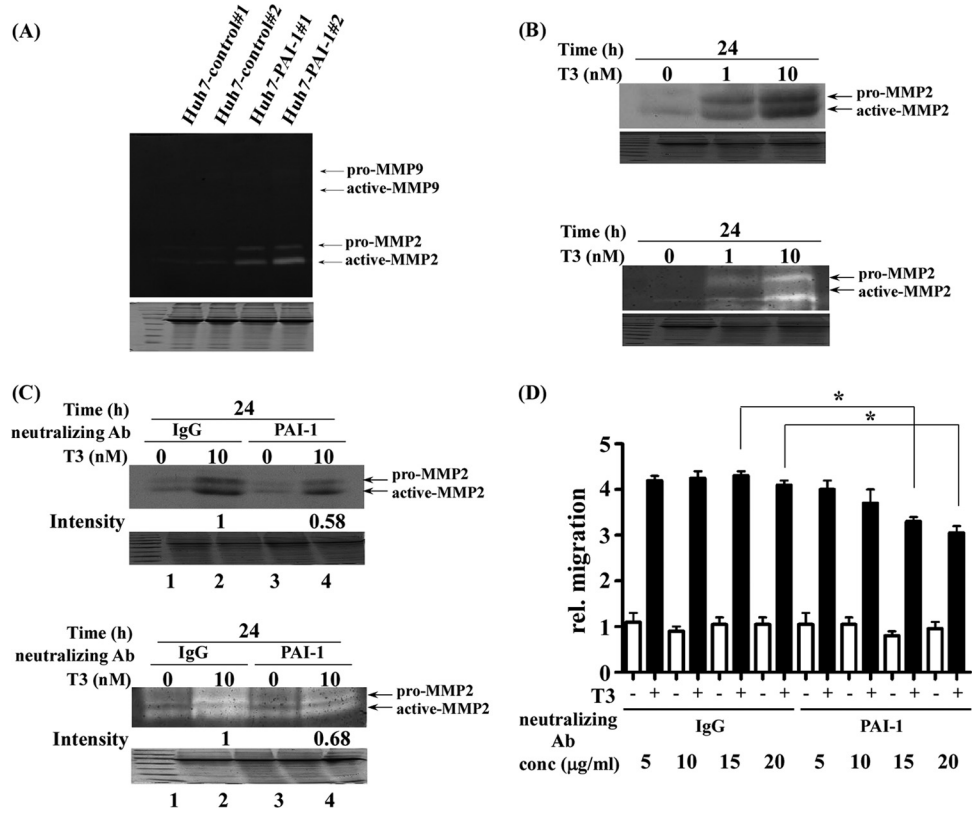

FIG. 8. **PAI-1 involved in the T_3-modulated migration pathways.** *A*, MMP activities of Huh7-control and Huh7-PAI-1 (4×10^6) stable lines were analyzed with the zymography assay, as described under "Experimental Procedures". The positions of proenzyme and active MMPs are indicated. *B*, MMP expression and activity of HepG2-TRα1 cells treated with or without 1 and 10 nM T_3 for 24h were analyzed with the (*B*, *upper* panel) Western blotting and (*B*, *lower* panel) zymography assay, as described under "Experimental Procedures." The positions of proenzyme and active MMPs are indicated. *C*, HepG2-TRα1 cells were pre-treated for 1 h with 15 μg/ml IgG and PAI-1 neutralizing antibody following treatment with T_3 (10 nM, 24h) or without (0 nM), and analyzed by (*C*, *upper* panel) Western blotting and (*C*, *lower* panel) zymography assay. *D*, J7-TRα1 cells (5×10^4) were seeded on the upper chamber of the transwell unit. J7-TRα1 cells in the upper chamber were incubated with serum-free medium, and the lower chamber contained 20% FBS DMEM. J7-TRα1 cells were pre-treated for 1 h with IgG and PAI-1 neutralizing antibody, following treatment with T_3 (10 nM, 24 h) or without (0 nM). The graph shows the number of filters with cells infiltrating the lower chamber from the upper chamber, providing an index of migration activity, as described under "Experimental Procedures." Values are shown as fold increase relative to the IgG control. Differences were analyzed using the Student's *t* test, $^*p < 0.05$.

active-MMP9 were not detected, even in PAI-1-overexpressing stable cells (Fig. 8*A*).

MMP2 activity and expression in response to T_3 treatment were assessed by Western blotting (Fig. 8*B*, *upper* panel) and zymography (Fig. 8*B*, *lower* panel). Such activity and expression were up-regulated by T_3, in a dose-dependent manner, in HepG2-TRα1 cells (Fig. 8). The influence of T_3 on MMP2 activity and expression was similar to that in cells overexpressing PAI-1 (Fig. 8*B*, *lower* panel *versus* Fig. 8*A*). In addition, we used an anti-PAI-1 antibody to explore whether PAI-1 was involved in T_3-mediated regulation of MMP2 activity. We found that anti-PAI-1 antibody reduced (~32–42%) the MMP2 expression (Fig. 8*C*, *upper* panel, lane 4 *versus* 2) and activity (Fig. 8*C*, *lower* panel, lane 4 *versus* 2) induced by T_3.

To further explore whether PAI-1 was involved in T_3-modulated cell migration, we performed an *in vitro* migration assay featuring addition of anti-PAI-1 (neutralizing) antibody at several concentrations after T_3 treatment. The migration ability gradually decreased in an anti-PAI-1 antibody concentration-dependent manner. Treatment with this antibody (20 μg/ml) reduced migration of J7-TRα1 cells by ~20–30% compared with that of control cells treated with IgG (Fig. 8*D*), suggesting that PAI-1 plays at least some role in T_3-mediated cell migration. Collectively, PAI-1 overexpression enhanced tumor growth and migration in a manner similar to what was seen when T_3 induced PAI-1 expression in J7-TRα1 cells, both *in vitro* and *in vivo*.

The Urokinase Plasminogen Activator System is Mediated by the Thyroid Hormone—The uPA system is activated in many cancers (26). In addition to PAI-1, urokinase plasminogen activator surface receptor (uPAR) and brain-specific serine protease 4 (BSSP4), involved in the uPA system (63), quantified in one of the three SILAC experiments, displayed a significant increase (T_3/Td >3) in T_3-treated HepG2-TRα1 cells (Table II). Protein and mRNA levels of uPAR and BSSP4 in conditioned media and extracts were validated using Western

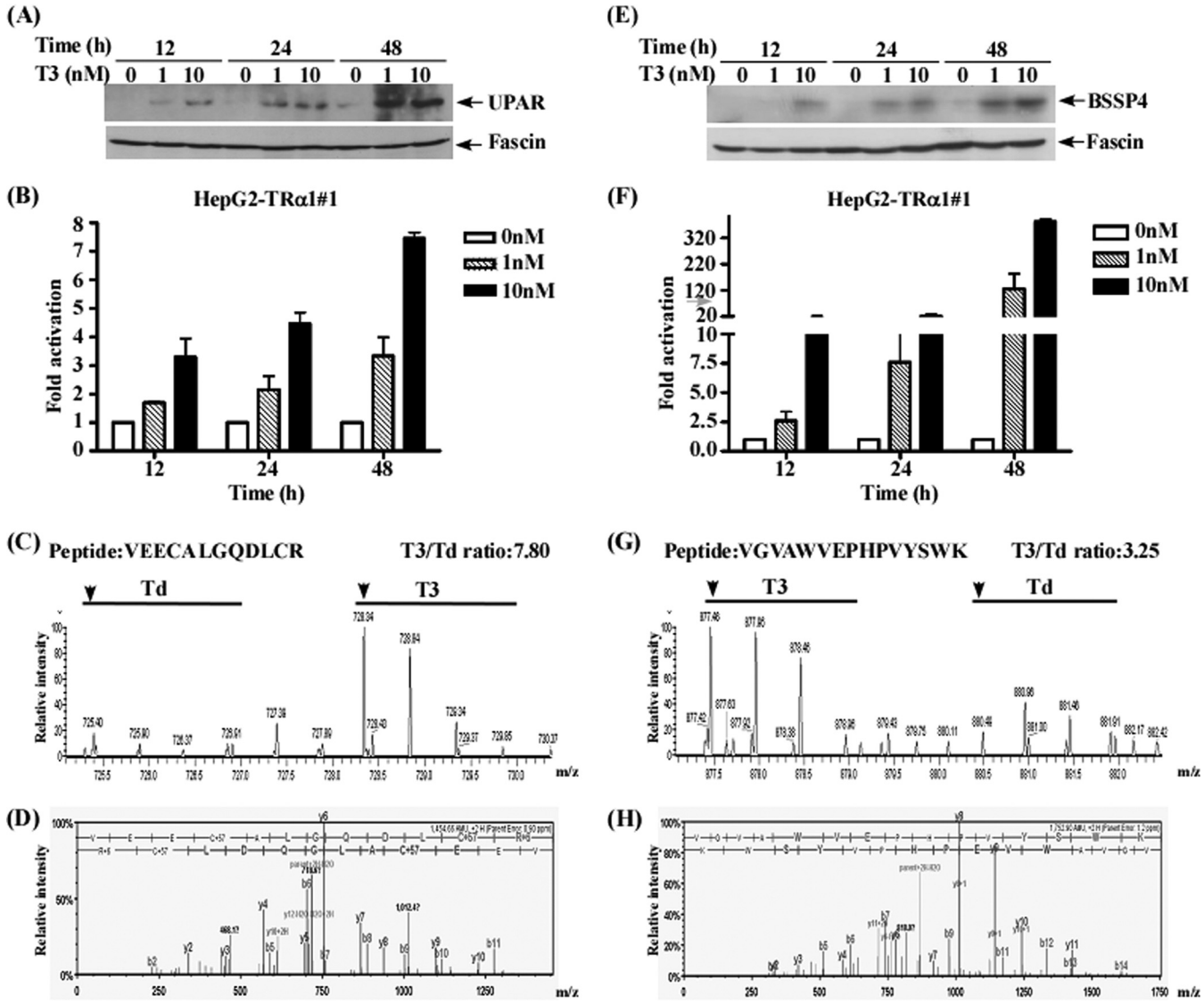

FIG. 9. **Validation of the proteins involved in the urokinase plasminogen activator system.** (*A*, *B*, *E*, *F*) Conditioned media and mRNA from HepG2-TRα1 cells treated with different T_3 concentrations (0, 1, 10 nM) for 12–48 h were analyzed using Western blot and Q- RT-PCR (uPAR, *A*, *B*; BSSP4, *E*, *F*). (*C*, *D*, *G*, *H*) Images showing MS spectra, MS/MS spectra, identified peptide sequences and quantified T_3/Td ratio (arrow head, first peak of the spectrum; T_3, 10 nM; Td, T_3-depleted) (uPAR, *C*, *D*; BSSP4, *G*, *H*).

blotting and quantitative RT-PCR, respectively. As shown in Figs. 9*A*, 9*B*, 9*E*, 9*F*, uPAR, BSSP4 protein and mRNA expression were increased in a time-course and dose-dependent manner following T_3 treatment. MS and MS/MS spectra of the representative peptides of each protein are presented in Figs. 9*C*, 9*D* and 9*G*, 9*H* to indicate the confidence of MS-based identification and quantification of these two proteins.

DISCUSSION

In this study, we have established the T_3-mediated HepG2-TRα1 secretome using a SILAC-based proteomics approach. Two protein/peptide separation techniques, GeLC and 2D-LC, were employed. Using the GeLC-MS/MS strategy, 635 proteins were identified, 56% of which were predicted using secretion pathway analyses. These results were comparative to the report of Wu *et al.* showing that 62.6% of the secreted proteins (485 of 775) identified in HepG2 cells could be predicted (31). In addition, up to 62% of secreted proteins coexisted in the two HepG2 secretome databases analyzed with the GeLC-MS/MS strategy. On the other hand, about 40% secreted proteins were only identified in one study, indicating that limitations of protein identification with the GeLC-MS/MS strategy exist for the HepG2 secretome. Therefore, LC-based peptide separation analysis, 2DLC-MS/MS, was performed. A comparable number of proteins were identified in two independent experiments (E2 and E3), specifically, 1508 proteins in E2 and 1350 in E3. Our results indicate that 2DLC-MS/MS is more effective than GeLC-MS/MS for the identification of proteins from the HepG2 secretome. In total, 1742 and 1714

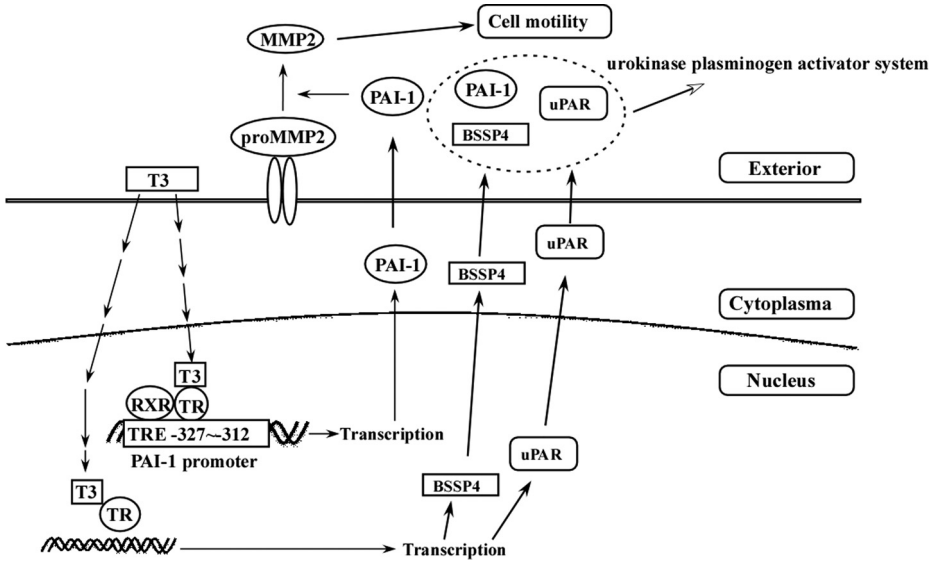

FIG. 10. **Schematic presentation of the pathway of TH-mediated migration and urokinase plasminogen activator system.** Addition of T_3 (10 nM) to HepG2-TRα1 cells activated PAI-1 expression via direct binding of TR proteins to TRE (–327~–312) of the PAI-1 promoter. MMP2 activity was altered in the presence of PAI-1 in Huh7 cells. PAI-1, uPAR and BSSP4 proteins, involved in the same pathway of the uPA system, were regulated by TH in SILAC-based experiments.

protein in the HepG2 secretome were identified and quantified, respectively. To our knowledge, this is the largest HepG2 secretome database reported to date.

We validated 12 candidates represented in three independent experiments (FIBG, FINC, FURIN, GELS, KNG1, PAI-1, SPON2, TIMP2, CADH2, FSCN1, uPAR and BSSP4) using Western blotting. These results further confirmed data obtained from SILAC-based analysis, supporting the theory that the SILAC strategy represents a powerful tool to investigate the T_3-mediated secretome. Furthermore, we identified 25 TH-regulated plasma proteins in the human HCC cell line using cDNA microarray (13). Among them, the current SILAC-based secretome mainly contained 21 including transferrin, prothrombin, fibrinogen, angiotensinogen, clusterin, haptoglobin, lipoprotein, and complement. Chan and co-workers reported some TH-regulated genes (angiopoietin-related protein 2, BHMT2, CDA7L, and ectonucleotide pyroph phatase/ph phodiesterase family member 2) related to cancer progression that were also identified in our SILAC-based dataset (64). CATH is slightly increased in the TH-regulated secretome (~1.61×) and overexpressed in numerous cancers, including glioma, melanoma, breast carcinoma, colorectal and prostate carcinoma (61, 65–68). Moreover, several tumor-associated genes, such as furin (FURIN) and gelsolin (GELS), are up-regulated by T_3 in the SILAC secretome (16, 69). The T_3-mediated secretome established in this study may thus provide a resource to explore TH-regulated tumor markers.

Recently, more reports have demonstrated the PAI-1 plays a crucial role in cancer cell survival and viability via alterations in the cell signaling pathway (70–72). PAI-1 has been previously identified, by two dimensional-PAGE, in the secretome of human HepG2 cells (73). PAI-1, one of the T_3 targets, was extensively characterized to elucidate the molecular mechanism of its regulation by T_3 in isogenic HepG2 cell lines. We have shown that T_3 induces *PAI-1* mRNA and protein expression in HepG2 and Huh7 cell lines expressing detectable endogenous TR proteins as well as in thyroidectomized rats. Further, it has been reported that thyroid hormones stimulate *PAI-1* mRNA expression in 3T3-L1 adipocytes, but the effect was not observed *in vivo* at either the mRNA or protein level in adipose tissue of T_4-treated rats (59). These findings suggest that adipocytes can respond in a diverse manner to thyroid hormones *in vitro* or *in vivo*. Further studies confirmed that T_3 up-regulates *PAI-1* at the transcription level, and TR and RXRα complexes directly bind TRE between positions –327/–312 of the *PAI-1* gene 5′-flanking region. Additionally, cell lines overexpressing PAI-1 showed higher migration and proliferation abilities, both *in vitro* and *in vivo*. Importantly, PAI-1 may aid in accelerating cell migration by abrogating the interactions between vitronectin and uPAR as well as plasmin and uPA, suggestive of vital roles in modulating cell adhesion and motility (74). The PAI-1-mediated migration was parallel with the enhancement of MMP2 activity, which was consistently with the previous report that PAI-1 plays as a crucial role to modulate matrix remodeling in extracellular space (75, 76). Collectively, these results suggest T_3 additionally promotes MMP activation, in parallel with PAI-1-mediated migration, by enhancing MMP2 activity. We speculate that PAI-1 is involved in T_3/TR-mediated liver cancer progression.

Clearly, T_3-mediated cell migration was significantly reduced upon addition of anti-PAI-1 antibody, but inhibition was not complete. *T_3* exerts *pleiotropic* effects on cell migration and metastasis mediated by several genes including non-

metastatic 23 (NM23) (77), FURIN (16), pituitary tumor-transforming 1 (PTTG1) (17), CATH (61), and methionine adenosyltransferase 1 (MATA1) (38); PAI-1 is only one of the known T_3-regulated targets. Additionally, MMP2 activity and expression were influenced by T_3 treatment in the present study; such an effect is therefore not unique to PAI-1. Extracellular PAI-1 activity, but not intracellular PAI-1 activity, can be abolished by neutralizing antibody. Therefore, T_3-mediated cell migration was partially inhibited by such an antibody.

In addition to PAI-1, uPAR and BSSP4 involved in the uPA system were also identified and quantified as TH-mediated targets in the SILAC-based analysis (Table II). The uPA system is a serine protease family (including tPA, uPA, uPAR, and PAIs) that is activated in many cancers and are frequently associated with cancer cell progression and high mortality (26). Moreover, Yasuda *et al.* showed the BSSP4, a novel member of the uPA system, is a serine protease that catalyzes the activation of inactive uPA (63). The sequence of events following activation with T_3 in SILAC-based experiments is depicted in Fig. 10. Taken together, we have successfully identified TH-regulated target genes involved in the uPA system using the SILAC-based strategy. Several genes implicated in cancer cell progression are altered by T_3, but the mechanism involved in TH-regulated secretion or signaling remains to be established. Our SILAC-based secretome dataset may be employed as a reference for determining the proteins involved in tumor progression and prognosis.

Acknowledgments—We have no conflicting financial interests.

* This work was supported by grants from Chang Gung Molecular Medicine Research Center, Taoyuan, Taiwan (CMRPD 170091-93, NMRP 140513, 170651-170653) and from the National Science Council of the Republic of China (NSC 96-2320-B-182-007, 97-2320-B-182-025-MY3).

S This article contains supplemental Tables S1 and S2.

‡‡ To whom correspondence should be addressed: Department of Biochemistry, Chang-Gung University, 259 Wen-hwa 1 Road, Taoyuan, Taiwan, Republic of China. Tel.: +886-3-2118263; E-mail: khlin@mail.cgu.edu.tw.

REFERENCES

1. Cheng, S. Y. (2000) Multiple mechanisms for regulation of the transcriptional activity of thyroid hormone receptors. *Rev. Endocr. Metab. Disord.* **1,** 9–18
2. Aranda, A., and Pascual, A. (2001) Nuclear hormone receptors and gene expression. *Physiol. Rev.* **81,** 1269–1304
3. Larsen, P. R. (2009) Thyroid hormone analogs and metabolites: new applications for an old hormone? *Nat. Clin. Pract. Endocrinol. Metab.* **5,** 1
4. Beato, M., Herrlich, P., and Schütz, G. (1995) Steroid hormone receptors: many actors in search of a plot. *Cell* **83,** 851–857
5. Lazar, M. A. (1993) Thyroid hormone receptors: multiple forms, multiple possibilities. *Endocr. Rev.* **14,** 184–193
6. Yen, P. M., and Chin, W. W. (1994) New advances in understanding the molecular mechanisms of thyroid hormone action. *Trends Endocrinol. Metab.* **5,** 65–72
7. Perlmann, T., Rangarajan, P. N., Umesono, K., and Evans, R. M. (1993) Determinants for selective RAR and TR recognition of direct repeat HREs. *Genes Dev.* **7,** 1411–1422
8. Yen, P. M., Ikeda, M., Wilcox, E. C., Brubaker, J. H., Spanjaard, R. A., Sugawara, A., and Chin, W. W. (1994) Half-site arrangement of hybrid glucocorticoid and thyroid hormone response elements specifies thyroid hormone receptor complex binding to DNA and transcriptional activity. *J. Biol. Chem.* **269,** 12704–12709
9. Yen, P. M. (2001) Physiological and molecular basis of thyroid hormone action. *Physiol. Rev.* **81,** 1097–1142
10. Wood, W. M., Dowding, J. M., Bright, T. M., McDermott, M. T., Haugen, B. R., Gordon, D. F., and Ridgway, E. C. (1996) Thyroid hormone receptor beta2 promoter activity in pituitary cells is regulated by Pit-1. *J. Biol. Chem.* **271,** 24213–24220
11. Chamba, A., Neuberger, J., Strain, A., Hopkins, J., Sheppard, M. C., and Franklyn, J. A. (1996) Expression and function of thyroid hormone receptor variants in normal and chronically diseased human liver. *J. Clin. Endocrinol. Metab.* **81,** 360–367
12. Lin, K. H., Chen, C. Y., Chen, S. L., Yen, C. C., Huang, Y. H., Shih, C. H., Shen, J. J., Yang, R. C., and Wang, C. S. (2004) Regulation of fibronectin by thyroid hormone receptors. *J. Mol. Endocrinol.* **33,** 445–458
13. Lin, K. H., Lee, H. Y., Shih, C. H., Yen, C. C., Chen, S. L., Yang, R. C., and Wang, C. S. (2003) Plasma protein regulation by thyroid hormone. *J. Endocrinol.* **179,** 367–377
14. Tai, P. J., Huang, Y. H., Shih, C. H., Chen, R. N., Chen, C. D., Chen, W. J., Wang, C. S., and Lin, K. H. (2007) Direct regulation of androgen receptor-associated protein 70 by thyroid hormone and its receptors. *Endocrinology* **148,** 3485–3495
15. Lin, K. H., Shieh, H. Y., and Hsu, H. C. (2000) Negative regulation of the antimetastatic gene Nm23-H1 by thyroid hormone receptors. *Endocrinology* **141,** 2540–2547
16. Chen, R. N., Huang, Y. H., Lin, Y. C., Yeh, C. T., Liang, Y., Chen, S. L., and Lin, K. H. (2008) Thyroid hormone promotes cell invasion through activation of furin expression in human hepatoma cell lines. *Endocrinology* **149,** 3817–3831
17. Chen, R. N., Huang, Y. H., Yeh, C. T., Liao, C. H., and Lin, K. H. (2008) Thyroid hormone receptors suppress pituitary tumor transforming gene 1 activity in hepatoma. *Cancer Res.* **68,** 1697–1706
18. Mohamed, M. M., and Sloane, B. F. (2006) Cysteine cathepsins: multifunctional enzymes in cancer. *Nat. Rev. Cancer* **6,** 764–775
19. Wilson, T. J., and Singh, R. K. (2008) Proteases as modulators of tumor-stromal interaction: primary tumors to bone metastases. *Biochim. Biophys. Acta* **1785,** 85–95
20. Hofmann, U. B., Eggert, A. A., Blass, K., Bröcker, E. B., and Becker, J. C. (2003) Expression of matrix metalloproteinases in the microenvironment of spontaneous and experimental melanoma metastases reflects the requirements for tumor formation. *Cancer Res.* **63,** 8221–8225
21. Piersma, S. R., Fiedler, U., Span, S., Lingnau, A., Pham, T. V., Hoffmann, S., Kubbutat, M. H., and Jiménez, C. R. (2010) Workflow comparison for label-free, quantitative secretome proteomics for cancer biomarker discovery: method evaluation, differential analysis, and verification in serum. *J. Proteome Res.* **9,** 1913–1922
22. Planque, C., Kulasingam, V., Smith, C. R., Reckamp, K., Goodglick, L., and Diamandis, E. P. (2009) Identification of five candidate lung cancer biomarkers by proteomics analysis of conditioned media of four lung cancer cell lines. *Mol. Cell. Proteomics* **8,** 2746–2758
23. Grønborg, M., Kristiansen, T. Z., Iwahori, A., Chang, R., Reddy, R., Sato, N., Molina, H., Jensen, O. N., Hruban, R. H., Goggins, M. G., Maitra, A., and Pandey, A. (2006) Biomarker discovery from pancreatic cancer secretome using a differential proteomic approach. *Mol. Cell. Proteomics* **5,** 157–171
24. Chenau, J., Michelland, S., de Fraipont, F., Josserand, V., Coll, J. L., Favrot, M. C., and Seve, M. (2009) The cell line secretome, a suitable tool for investigating proteins released in vivo by tumors: application to the study of p53-modulated proteins secreted in lung cancer cells. *J. Proteome Res.* **8,** 4579–4591
25. Mathias, R. A., Wang, B., Ji, H., Kapp, E. A., Moritz, R. L., Zhu, H. J., and Simpson, R. J. (2009) Secretome-based proteomic profiling of Ras-transformed MDCK cells reveals extracellular modulators of epithelial-mesenchymal transition. *J. Proteome Res.* **8,** 2827–2837
26. Dass, K., Ahmad, A., Azmi, A., Sarkar, S., and Sarkar, F. (2008) Evolving role of uPA/uPAR system in human cancers. *Cancer Treatment Rev.* **34,** 122–136
27. Samuels, H. H., Stanley, F., and Casanova, J. (1979) Depletion of L-3,5,3′-triiodothyronine and L-thyroxine in euthyroid calf serum for use in cell culture studies of the action of thyroid hormone. *Endocrinology* **105,**

80–85
28. Ong, S. E., and Mann, M. (2006) A practical recipe for stable isotope labeling by amino acids in cell culture (SILAC). *Nat. Protoc.* **1,** 2650–2660
29. Wu, C. C., Chen, H. C., Chen, S. J., Liu, H. P., Hsieh, Y. Y., Yu, C. J., Tang, R., Hsieh, L. L., Yu, J. S., and Chang, Y. S. (2008) Identification of collapsin response mediator protein-2 as a potential marker of colorectal carcinoma by comparative analysis of cancer cell secretomes. *Proteomics* **8,** 316–332
30. Li, Y., Yu, J., Wang, Y., Griffin, N. M., Long, F., Shore, S., Oh, P., and Schnitzer, J. E. (2009) Enhancing identifications of lipid-embedded proteins by mass spectrometry for improved mapping of endothelial plasma membranes in vivo. *Mol. Cell. Proteomics* **8,** 1219–1235
31. Wu, C. C., Hsu, C. W., Chen, C. D., Yu, C. J., Chang, K. P., Tai, D. I., Liu, H. P., Su, W. H., Chang, Y. S., and Yu, J. S. (2010) Candidate serological biomarkers for cancer identified from the secretomes of 23 cancer cell lines and the human protein atlas. *Mol. Cell. Proteomics* **9,** 1100–1117
32. Cox, J., and Mann, M. (2008) MaxQuant enables high peptide identification rates, individualized p.p.b.-range mass accuracies and proteome-wide protein quantification. *Nat. Biotechnol.* **26,** 1367–1372
33. Cox, J., Matic, I., Hilger, M., Nagaraj, N., Selbach, M., Olsen, J. V., and Mann, M. (2009) A practical guide to the MaxQuant computational platform for SILAC-based quantitative proteomics. *Nat. Protoc.* **4,** 698–705
34. Bendtsen, J. D., Nielsen, H., von Heijne, G., and Brunak, S. (2004) Improved prediction of signal peptides: SignalP 3.0. *J. Mol. Biol.* **340,** 783–795
35. Bendtsen, J. D., Jensen, L. J., Blom, N., Von Heijne, G., and Brunak, S. (2004) Feature-based prediction of non-classical and leaderless protein secretion. *Protein Eng. Des. Sel.* **17,** 349–356
36. Möller, S., Croning, M. D., and Apweiler, R. (2001) Evaluation of methods for the prediction of membrane spanning regions. *Bioinformatics* **17,** 646–653
37. Liao, C. H., Yeh, S. C., Huang, Y. H., Chen, R. N., Tsai, M. M., Chen, W. J., Chi, H. C., Tai, P. J., Liao, C. J., Wu, S. M., Cheng, W. L., Pai, L. M., and Lin, K. H. (2010) Positive regulation of spondin 2 by thyroid hormone is associated with cell migration and invasion. *Endocrine Related Cancer* **17,** 99–111
38. Wu, S. M., Huang, Y. H., Lu, Y. H., Chien, L. F., Yeh, C. T., Tsai, M. M., Liao, C. H., Chen, W. J., Liao, C. J., Cheng, W. L., and Lin, K. H. (2010) Thyroid hormone receptor-mediated regulation of the methionine adenosyltransferase 1 gene is associated with cell invasion in hepatoma cell lines. *Cell. Mol. Life Sci.* **67,** 1831–1843
39. Huang, Y. H., Lee, C. Y., Tai, P. J., Yen, C. C., Liao, C. Y., Chen, W. J., Liao, C. J., Cheng, W. L., Chen, R. N., Wu, S. M., Wang, C. S., and Lin, K. H. (2006) Indirect regulation of human dehydroepiandrosterone sulfotransferase family 1A member 2 by thyroid hormones. *Endocrinology* **147,** 2481–2489
40. Repesh, L. A. (1989) A new in vitro assay for quantitating tumor cell invasion. *Invasion Metastasis* **9,** 192–208
41. Shih, C. H., Chen, S. L., Yen, C. C., Huang, Y. H., Chen, C. D., Lee, Y. S., and Lin, K. H. (2004) Thyroid hormone receptor-dependent transcriptional regulation of fibrinogen and coagulation proteins. *Endocrinology* **145,** 2804–2814
42. Martínez-Iglesias, O., Garcia-Silva, S., Regadera, J., and Aranda, A. (2009) Hypothyroidism enhances tumor invasiveness and metastasis development. *PLoS One* **4,** e6428
43. Kowalik, M. A., Perra, A., Pibiri, M., Cocco, M. T., Samarut, J., Plateroti, M., Ledda-Columbano, G. M., and Columbano, A. (2010) TRbeta is the critical thyroid hormone receptor isoform in T3-induced proliferation of hepatocytes and pancreatic acinar cells. *J. Hepatol.* **53,** 686–692
44. Benvenga, S., Cahnmann, H. J., Rader, D., Kindt, M., Facchiano, A., and Robbins, J. (1994) Thyroid hormone binding to isolated human apolipoproteins A-II, C-I, C-II, and C-III: homology in thyroxine binding sites. *Thyroid* **4,** 261–267
45. Lin-Lee, Y. C., Strobl, W., Soyal, S., Radosavljevic, M., Song, M., Gotto, A. M., Jr., and Patsch, W. (1993) Role of thyroid hormone in the expression of apolipoprotein A-IV and C-III genes in rat liver. *J. Lipid Res.* **34,** 249–259
46. Prieur, X., Huby, T., Coste, H., Schaap, F. G., Chapman, M. J., and Rodríguez, J. C. (2005) Thyroid hormone regulates the hypotriglyceridemic gene APOA5. *J. Biol. Chem.* **280,** 27533–27543
47. Kardassis, D., Roussou, A., Papakosta, P., Boulias, K., Talianidis, I., and Zannis, V. I. (2003) Synergism between nuclear receptors bound to specific hormone response elements of the hepatic control region-1 and the proximal apolipoprotein C-II promoter mediate apolipoprotein C-II gene regulation by bile acids and retinoids. *Biochem. J.* **372,** 291–304
48. Lambrinoudaki, I., Kaparos, G., Rizos, D., Galapi, F., Alexandrou, A., Sergentanis, T. N., Creatsa, M., Christodoulakos, G., Kouskouni, E., and Botsis, D. (2009) Apolipoprotein E and paraoxonase 1 polymorphisms are associated with lower serum thyroid hormones in postmenopausal women. *Clin. Endocrinol.* **71,** 284–290
49. Izaguirre, M. F., and Casco, V. H. (2010) T3 regulates E-cadherin, and beta- and alpha-catenin expression in the stomach during the metamorphosis of the toad Rhinella arenarum. *Biotech. Histochem.* **85,** 305–323
50. Rigaud, D., Tallonneau, I., and Vergès, B. (2009) Hypercholesterolaemia in anorexia nervosa: frequency and changes during refeeding. *Diabetes Metab.* **35,** 57–63
51. Varga, F., Rumpler, M., Zoehrer, R., Turecek, C., Spitzer, S., Thaler, R., Paschalis, E. P., and Klaushofer, K. (2010) T3 affects expression of collagen I and collagen cross-linking in bone cell cultures. *Biochem. Biophys. Res. Commun.* **402,** 180–185
52. Haas, M. J., Mreyoud, A., Fishman, M., and Mooradian, A. D. (2004) Microarray analysis of thyroid hormone-induced changes in mRNA expression in the adult rat brain. *Neurosci. Lett.* **365,** 14–18
53. Cakal, B., Cakal, E., Demirbas, B., Ozkaya, M., Karaahmetoğlu, S., Serter, R., and Aral, Y. (2007) Homocysteine and fibrinogen changes with L-thyroxine in subclinical hypothyroid patients. *J. Korean Med. Sci.* **22,** 431–435
54. Ventura-Holman, T., Mamoon, A., Subauste, M. C., and Subauste, J. S. (2011) The effect of oncoprotein v-erbA on thyroid hormone-regulated genes in hepatocytes and their potential role in hepatocellular carcinoma. *Mol. Biol. Rep.* **38,** 1137–1144
55. Zhao, L. N., Xu, J., Peng, X. L., Tian, L. Y., Hao, L. P., Yang, X. F., Ying, C. J., and Sun, X. F. (2010) Dose and time-dependent hypercholesterolemic effects of iodine excess via TRbeta1-mediated down regulation of hepatic LDLr gene expression. *Eur. J. Nutr.* **49,** 257–265
56. Erem, C., Ersoz, H. O., Karti, S. S., Ukinc, K., Hacihasanoglu, A., Değer, O., and Telatar, M. (2002) Blood coagulation and fibrinolysis in patients with hyperthyroidism. *J. Endocrinol. Invest.* **25,** 345–350
57. Erem, C., Ucuncu, O., Yilmaz, M., Kocak, M., Nuhoglu, I., and Ersoz, H. O. (2009) Increased thrombin-activatable fibrinolysis inhibitor and decreased tissue factor pathway inhibitor in patients with hypothyroidism. *Endocrine* **35,** 75–80
58. Beazley, K. E., Canner, J. P., and Linsenmayer, T. F. (2009) Developmental regulation of the nuclear ferritoid-ferritin complex of avian corneal epithelial cells: roles of systemic factors and thyroxine. *Exp. Eye Res.* **89,** 854–862
59. Biz, C., Oliveira, C., Mattos, A. B., Oliveira, J., Ribeiro, E. B., Oller do Nascimento, C. M., and Oyama, L. M. (2009) The effect of thyroid hormones on the white adipose tissue gene expression of PAI-1 and its serum concentration. *Braz. J. Med. Biol. Res.* **42,** 1163–1166
60. Nikolsky, Y., Ekins, S., Nikolskaya, T., and Bugrim, A. (2005) A novel method for generation of signature networks as biomarkers from complex high throughput data. *Toxicol. Lett.* **158,** 20–29
61. Wu, S. M., Huang, Y. H., Yeh, C. T., Tsai, M. M., Liao, C. H., Cheng, W. L., Chen, W. J., and Lin, K. H. (2011) Cathepsin H regulated by the thyroid hormone receptors associate with tumor invasion in human hepatoma cells. *Oncogene*
62. Gomis-Rüth, F. X. (2003) Structural aspects of the metzincin clan of metalloendopeptidases. *Mol. Biotechnol.* **24,** 157–202
63. Yasuda, S., Morokawa, N., Wong, G. W., Rossi, A., Madhusudhan, M. S., Sali, A., Askew, Y. S., Adachi, R., Silverman, G. A., Krilis, S. A., and Stevens, R. L. (2005) Urokinase-type plasminogen activator is a preferred substrate of the human epithelium serine protease tryptase epsilon/PRSS22. *Blood* **105,** 3893–3901
64. Chan, I. H., and Privalsky, M. L. (2009) Thyroid hormone receptor mutants implicated in human hepatocellular carcinoma display an altered target gene repertoire. *Oncogene* **28,** 4162–4174
65. del Re, E. C., Shuja, S., Cai, J., and Murnane, M. J. (2000) Alterations in cathepsin H activity and protein patterns in human colorectal carcinomas. *Br. J. Cancer* **82,** 1317–1326
66. Sivaparvathi, M., Sawaya, R., Gokaslan, Z. L., Chintala, S. K., Rao, J. S., and Chintala, K. S. (1996) Expression and the role of cathepsin H in human glioma progression and invasion. *Cancer Lett.* **104,** 121–126

67. Kos, J., Stabuc, B., Schweiger, A., Krasovec, M., Cimerman, N., Kopitar-Jerala, N., and Vrhovec, I. (1997) Cathepsins B, H, and L and their inhibitors stefin A and cystatin C in sera of melanoma patients. *Clin. Cancer Res.* **3,** 1815–1822
68. Gabrijelcic, D., Svetic, B., Spaić, D., Skrk, J., Budihna, M., Dolenc, I., Popovic, T., Cotic, V., and Turk, V. (1992) Cathepsins B, H and L in human breast carcinoma. *Eur. J. Clin. Chem. Clin. Biochem.* **30,** 69–74
69. Liao, C. J., Wu, T. I., Huang, Y. H., Chang, T. C., Wang, C. S., Tsai, M. M., Hsu, C. Y., Tsai, M. H., Lai, C. H., and Lin, K. H. (2011) Overexpression of gelsolin in human cervical carcinoma and its clinicopathological significance. *Gynecol. Oncol.* **120,** 135–144
70. Webb, D. J., Thomas, K. S., and Gonias, S. L. (2001) Plasminogen activator inhibitor 1 functions as a urokinase response modifier at the level of cell signaling and thereby promotes MCF-7 cell growth. *J. Cell Biol.* **152,** 741–752
71. Romer, M. U., Larsen, L., Offenberg, H., Brünner, N., and Lademann, U. A. (2008) Plasminogen activator inhibitor 1 protects fibrosarcoma cells from etoposide-induced apoptosis through activation of the PI3K/Akt cell survival pathway. *Neoplasia* **10,** 1083–1091
72. Bajou, K., Peng, H., Laug, W. E., Maillard, C., Noel, A., Foidart, J. M., Martial, J. A., and DeClerck, Y. A. (2008) Plasminogen activator inhibitor-1 protects endothelial cells from FasL-mediated apoptosis. *Cancer Cell* **14,** 324–334
73. Slany, A., Haudek, V. J., Zwickl, H., Gundacker, N. C., Grusch, M., Weiss, T. S., Seir, K., Rodgarkia-Dara, C., Hellerbrand, C., and Gerner, C. (2010) Cell characterization by proteome profiling applied to primary hepatocytes and hepatocyte cell lines Hep-G2 and Hep-3B. *J. Proteome Res.* **9,** 6–21
74. Waltz, D. A., Natkin, L. R., Fujita, R. M., Wei, Y., and Chapman, H. A. (1997) Plasmin and plasminogen activator inhibitor type 1 promote cellular motility by regulating the interaction between the urokinase receptor and vitronectin. *J. Clin. Invest.* **100,** 58–67
75. Collen, D. (1999) The plasminogen (fibrinolytic) system. *Thromb. Haemost.* **82,** 259–270
76. Andreasen, P. A., Georg, B., Lund, L. R., Riccio, A., and Stacey, S. N. (1990) Plasminogen activator inhibitors: hormonally regulated serpins. *Mol. Cell. Endocrinol.* **68,** 1–19
77. Lin, K. H., Lin, Y. W., Lee, H. F., Liu, W. L., Chen, S. T., Chang, K. S., and Cheng, S. Y. (1995) Increased invasive activity of human hepatocellular carcinoma cells is associated with an overexpression of thyroid hormone beta 1 nuclear receptor and low expression of the anti-metastatic nm23 gene. *Cancer Lett.* **98,** 89–95